AGU PUBLICATIONS

JGR

Journal of Geophysical Research: Atmospheres

RESEARCH ARTICLE
10.1002/2017JD026872

Key Points:
- Primary marine aerosol production is modulated by surface-active organic matter in the seawater
- Primary marine aerosol production varies based on seawater type, bubble plume dynamics, and characteristics of the air-water interface
- Organic enrichments and mass fractions of fresh marine aerosol are relatively invariant over broad ranges of physicochemical conditions

Supporting Information:
- Supporting Information S1

Correspondence to:
W. C. Keene,
wck@virginia.edu

Citation:
Keene, W. C., Long, M. S., Reid, J. S., Frossard, A. A., Kieber, D. J., Maben, J. R., … Bates, T. S. (2017). Factors that modulate properties of primary marine aerosol generated from ambient seawater on ships at sea. *Journal of Geophysical Research: Atmospheres*, *122*, 11,961–11,990. https://doi.org/10.1002/2017JD026872

Received 29 MAR 2017
Accepted 12 OCT 2017
Accepted article online 19 OCT 2017
Published online 9 NOV 2017

Factors That Modulate Properties of Primary Marine Aerosol Generated From Ambient Seawater on Ships at Sea

William C. Keene[1], Michael S. Long[2], Jeffrey S. Reid[3], Amanda A. Frossard[4,5], David J. Kieber[6], John R. Maben[1], Lynn M. Russell[4], Joanna D. Kinsey[6,7], Patricia K. Quinn[8], and Timothy S. Bates[9]

[1]Department of Environmental Sciences, University of Virginia, Charlottesville, VA, USA, [2]John A. Paulson School of Engineering and Applied Sciences, Harvard University, Cambridge, MA, USA, [3]Naval Research Laboratory, Monterey, CA, USA, [4]Scripps Institution of Oceanography, University of California, San Diego, La Jolla, CA, USA, [5]Now at Department of Chemistry, University of Georgia, Athens, GA, USA, [6]Department of Chemistry, State University of New York, College of Environmental Science and Forestry, Syracuse, NY, USA, [7]Now at Department of Marine, Earth, and Atmospheric Sciences, North Carolina State University at Raleigh, Raleigh, NC, USA, [8]Pacific Marine Environmental Laboratory, NOAA, Seattle, WA, USA, [9]Joint Institute for the Study of the Atmosphere and Ocean, University of Washington, Seattle, WA, USA

Abstract Model primary marine aerosol (mPMA) was produced by bubbling clean air through flowing natural seawater in a high-capacity generator deployed on ships in the eastern North Pacific and western North Atlantic Oceans. Physicochemical properties of seawater and mPMA were quantified to characterize factors that modulated production. Differences in surfactant organic matter (OM) and associated properties including surface tension sustained plumes with smaller bubble sizes, slower rise velocities, larger void fractions, and older surface ages in biologically productive relative to oligotrophic seawater. Production efficiencies for mPMA number (PE_{num}) and mass (PE_{mass}) per unit air detrained from biologically productive seawater during daytime were greater and mass median diameters smaller than those in the same seawater at night and in oligotrophic seawater during day and night. PE_{mass} decreased with increasing air detrainment rate suggesting that surface bubble rafts suppressed emission of jet droplets and associated mPMA mass. Relative to bubbles emitted at 60 cm depth, PE_{num} for bubbles emitted from 100 cm depth was approximately 2 times greater. mPMA OM enrichment factors (EFs) and mass fractions based on a coarse frit, fine frits, and a seawater jet exhibited similar size-dependent variability over a wide range in chlorophyll *a* concentrations. Results indicate that the physical production of PMA number and mass from the ocean surface varies systematically as interrelated functions of seawater type and, in biologically productive waters, time of day; bubble injection rate, depth, size, and surface age; and physical characteristics of the air-water interface whereas size-resolved OM EFs and mass fractions are relatively invariant.

1. Introduction

The production, physicochemical processing, and environmental implications of marine aerosol have been actively investigated since the midtwentieth century (e.g., Blanchard, 1963; Blanchard & Woodcock, 1980; Boyce, 1954; Monahan, 1968; Woodcock, 1953; Woodcock & Gifford, 1949). It is widely recognized that the production of marine aerosol particles at the ocean surface drives important geochemical cycles (Duce et al., 1965; Eriksson, 1960; Long, Keene, Easter, et al., 2014; Sander et al., 2003), influences the nature of marine clouds and precipitation (e.g., Beard & Ochs, 1993; Feingold et al., 1999; Levin et al., 2005; Szumowski et al., 1999; Woodcock, 1952), and is the dominant source of aerosol that modulates radiative properties of the troposphere (e.g., Haywood et al., 1999; Murphy et al., 1998). However, despite this well-known importance, reliable prediction of size- and composition-resolved production fluxes of primary marine aerosol (PMA) and the associated impacts on the marine troposphere and climate remains problematic. For example, relative differences between aerosol characteristics measured in situ (Reid et al., 2006) and remotely sensed (e.g., Myhre et al., 2005, 2004; Zhang & Reid, 2006) over the open ocean are typically much greater than those in other regions or for terrestrial aerosol species. Large uncertainties associated with the representativeness of observations contribute to the order of magnitude or more divergence in modeled concentrations and fluxes of marine aerosol (e.g., Andreas, 1998; de Leeuw et al., 2011; Lewis & Schwartz, 2004; Sessions

et al., 2015). This divergence is substantially greater than corresponding divergence for other aerosol types (e.g., Sessions et al., 2015; Textor et al., 2006).

Central to the major sources of uncertainty in marine aerosol prediction is the complexity of the marine system itself. Marine aerosol generation, transport, and deposition as a function of size vary in response to interrelated dependencies of wind and wave fields, stability, turbulence, and sea surface temperature and chemistry (Callaghan et al., 2008; Lafon et al., 2007; Long, Keene, Kieber, et al., 2014; Mårtensson et al., 2003; Terrill et al., 2001). Marine boundary layers are typically only 500 to 1,000 m in vertical height with centimeter-scale interfaces and meter-scale layers at the sea surface that are not resolvable in mesoscale and global-scale models and are, thus, either highly parameterized or ignored. In addition, biological and physicochemical processes modulate the surface-active organic compounds in seawater that rapidly adsorb onto surfaces of freshly produced bubbles forming organic films that mediate processes controlling particle formation and associated chemical composition (Adamson & Gast, 1990; Lewis & Schwartz, 2004; Long, Keene, Kieber, et al., 2014; Modini et al., 2013; Prather et al., 2013). Surface-active compounds associated with the large and ubiquitous reservoir of old recalcitrant dissolved organic carbon (RDOC) in the surface ocean also adsorb onto bubble surfaces that modulate marine aerosol production and may account for significant fractions of the particulate organic material emitted to the atmosphere by breaking waves (Kieber et al., 2016). Reliable measurements at higher wind speeds in marine environments are quite challenging and sometimes impossible, which (coupled with the expense of ship time) has resulted in many data sets that are weighted disproportionately by observations in coastal regions and at lower winds speeds. Consequently, available data are probably not representative of the fully developed environment over the open ocean (Lafon et al., 2007). It is evident from the above that much of the variability among data sets and models alike arises from unmeasured or unaccounted for dependencies.

A second consideration relates to challenges in reliably characterizing the properties and sources of aerosols in the marine boundary layer (MBL). For example, incomplete (i.e., truncated to $PM_{2.5}$ or PM_{10}) and nonquantitative sampling (e.g., inertial segregation of particles at inlets and internal losses to surfaces) involving the upper end of the marine aerosol size distribution has resulted in large divergence among measured concentrations and estimated fluxes of size-resolved and total marine aerosol mass (Porter & Clarke, 1997; Reid et al., 2006; Reid & Peters, 2007). Environmental dependencies also arise from aerosol life cycles within the MBL. Anthropogenic sources of submicron diameter particles can significantly impact even the most remote marine environments (e.g., Clarke et al., 2013; Reid et al., 2013; Shank et al., 2012). In addition, atmospheric lifetimes of marine aerosols vary from many days to a week or more for submicron size fractions to hours for the upper end of the size distribution greater than about 5 μm diameter (Erickson et al., 1999; Reid et al., 2006, 2001). The chemical composition of freshly produced PMA also evolves rapidly in the atmosphere via interrelated processes including acidification, halogen activation, and organic photochemistry (e.g., Keene et al., 1998; Sander et al., 2003; Turekian et al., 2003; Zhou et al., 2008), and thus, aerosol composition is not conservative. Consequently, characteristics of marine aerosols measured at a given location and time are not representative of the corresponding PMA produced at that location and time or at any other location and time; it is not possible to reliably infer an initial condition based on measured characteristics of the ambient aerosol population.

Limitations in the marine system's observability has led to use of highly empirical relationships to predict size-resolved production fluxes of PMA, size-resolved concentrations of ambient marine aerosol, and aerosol optical thicknesses as functions of near-surface wind speed and whitecap coverage (Andreas, 1998; Clarke et al., 2006; Gong, 2003; Mårtensson et al., 2003; Monahan & O'Muircheartaigh, 1986; Smirnov et al., 2012; Tyree et al., 2007; Vignati et al., 2001) or wave-energy dissipation (Long et al., 2011; Norris et al., 2013). However, research spanning several decades has failed to resolve details of mechanistic interactions among sea state, surface ocean biogeochemistry, seawater organic matter (OM), and PMA production and composition (Gantt & Meskhidze, 2013; Gaston et al., 2011; Hoffman & Duce, 1976; Long et al., 2011; Meskhidze et al., 2013; O'Dowd et al., 2004, 2008). Recently, development of marine aerosol generation systems capable of producing model PMA (mPMA) from natural seawater under controlled conditions coupled with instrumentation to characterize corresponding chemical and physical properties over the full relevant size distribution has advanced mechanistic understanding of underlying processes (Facchini et al., 2008; Keene et al., 2007; Kieber et al., 2016; Long, Keene, Kieber, et al., 2014; Quinn et al., 2014).

The ultimate goals of our work are to (1) reliably characterize the properties and fluxes of freshly produced marine aerosol over the full relevant size range as functions of the major physical, chemical, and biological drivers and (2) employ these data to develop representative parameterizations of PMA production as functions of major drivers for application in models. In this paper, we present an integrated assessment of results for an in situ synthetic PMA generator as described in Keene et al. (2007) and Long, Keene, Kieber, et al. (2014) that was deployed during two oceanic cruises—one each in the eastern North Pacific and the western North Atlantic Oceans. We evaluate the major physical, chemical, and biological factors and associated interactions among factors that modulate mPMA production including bubble size and plume depth, air detrainment rate, solar radiation, the trophic status of seawater, and the concentration of dissolved organic carbon (DOC). Influences and limitations of generator design in simulating PMA production are discussed. Results provide relevant context for interpreting the representativeness and comparability of mPMA production based on different approaches and, ultimately, for improving the design of marine aerosol generation systems.

Several previous studies have evaluated variability in mPMA characteristics and production fluxes as functions of seawater properties and time of day based on subsets of data generated during these cruises (Bates et al., 2012; Frossard et al., 2014; Kieber et al., 2016; Long, Keene, Kieber, et al., 2014; Quinn et al., 2014). The following analysis considers a broader range of both environmental and operational factors that modulate mPMA production based on all relevant data from both campaigns, including results from previously unreported characterization experiments. Although some of our interpretations draw on previously published results, unless otherwise noted, results reported herein have either not been published previously or represent more comprehensive evaluations of data that had been presented previously in only summary form.

2. Methods

2.1. Cruise Tracks and Timing

mPMA emissions from biologically productive waters of the eastern North Pacific Ocean along the California coast (32.7°N to 38.6°N) were investigated during a cruise of the R/V *Atlantis* as part of the California Nexus (CalNex) campaign from 15 May to 7 June 2010. mPMA emissions from both biologically productive and oligotrophic regions of the western Atlantic Ocean were also investigated during a cruise of the R/V *Ronald H. Brown* as part of the Western Atlantic Climate Study (WACS) from 19 to 27 August 2012. During WACS, emission from biologically productive waters on Georges Bank, approximately 170 km east of Boston (~41.9°N, 67.4°W), was characterized from 20 to 23 August (hereafter referred to as WACS Station 1 or WACS-S1). Emission from oligotrophic waters in the Sargasso Sea (~36.3°N, 64.7°W) was characterized from 24 to 26 August (hereafter referred to as WACS Station 2 or WACS-S2). Figure 1 in Quinn et al. (2014) depicts the cruise tracks for both campaigns superimposed on the corresponding chlorophyll *a* (Chl *a*) concentrations.

2.2. mPMA Generator

mPMA was produced in a high-capacity generator fabricated from Pyrex and Teflon. The reader is referred to Keene et al. (2007) for a detailed description and schematic of the device and to Long, Keene, Kieber, et al. (2014) for an explanation of modifications implemented for deployment on ships at sea. Briefly, the 20 cm diameter generator consisted of a 122 cm deep seawater reservoir underlying a 97 cm deep atmosphere. Fresh seawater drawn from approximately 5 m depth through the ship's clean seawater line flowed into the base of the seawater reservoir (typically at 4 L min^{-1} yielding an upwelling velocity of 0.22 cm s^{-1}) and drained evenly over the top annular rim thereby continuously replacing the seawater surface and minimizing formation of standing bubble rafts. Bubbles were generated by two mechanisms. First, bubble plumes were produced by pumping ultrapure air through a coarse porosity sintered glass frit (45 mm diameter, 145 to 174 μm pore size) or through 11 fine porosity sintered glass frits (90 mm diameter, 10 to 20 μm pore size) positioned at an average depth of 84 cm below the air-seawater interface, which is within the range of ambient bubble cloud depths generated by breaking waves on the open-ocean surface (Thorpe, 1982; Thorpe & Hall, 1983; Thorpe et al., 1982). The fine frits were plumbed as two independently regulated sets of five and six frits each that were positioned at average depths of approximately 60 and 100 cm, respectively. To prevent flooding via backflow of seawater into the bubble air feed lines, it was necessary to maintain finite positive

pressure behind and associated minimal air flow of 0.2 L min^{-1} through the course frit and each set of fine frits (total of 0.6 L min^{-1} corresponding to an air detrainment rate of 0.31 L m^{-2} s^{-1}). The implications of background bubble production via this minimal air flow through the frits are discussed in more detail below. Second, bubble plumes were also produced by one or two seawater jets at combined flow rates of 1 to 4 L min^{-1} that impinged on the air-seawater interface. Jet nozzles were 0.32 cm ID and positioned at 50 cm above the interface.

mPMA was emitted to the headspace when bubbles rose to and burst at the air-seawater interface. Ultrapure sweep air flowed through the headspace above the seawater reservoir at 48 to 70 L min^{-1} (depending on the combined flow rates required to accommodate different sampling devices). Unless otherwise noted, sweep air was hydrated to a relative humidity (RH) of 80 ± 2%.

The generator was blank tested during both campaigns by measuring mPMA number concentrations in the headspace (using methods described below) at typical flow rates of bubble and sweep air but with no seawater in the reservoir. All blank tests yielded undetectable particle number concentrations (less than 2 cm^{-3}), indicating that all particles measured during routine operation originated from seawater.

2.3. Physical and Chemical Properties of Seawater

Measurement techniques for characteristics of seawater, solar radiation, and mPMA are reported in detail by Long, Keene, Kieber, et al. (2014). Briefly, temperature and salinity (ship's thermosalinograph) and Chl *a* concentrations (Turner model 10 AU fluorometer) in seawater and incident solar radiation (Epply models 8–48 and precision spectral pyranometers) were measured continuously. Dissolved organic carbon (DOC) in gravity-filtered seawater (0.2 μm Whatman POLYCAP 75 AS cartridge) was measured with a Shimadzu Model TOC-V CSH carbon analyzer. The dynamic surface tension of seawater (also referred to as bubble surface tension) was measured only during WACS with a Sensadyne Model QC-6000 bubble tensiometer. Bubble sizes at a depth of ~4 to 5 cm below the air-water interface within the generator were quantified using computer-enhanced camera images.

Steady state void fractions (volume of bubble air in the water column divided by the volume of the water column) were characterized for coarse- and fine-porosity frits in each seawater type over a range of air detrainment rates. Briefly, with the flow of bubble air set to the minimal rate (0.6 L min^{-1}) necessary to prevent backflow of seawater through the frits, the model ocean was completely filled with fresh seawater and then the seawater flow was turned off. For each set of conditions, the flow rate of bubble air was incrementally increased and the corresponding total volume of water displaced by bubble air was measured. The minimal bubble rate required to prevent backflow through the frits sustained a minor background air volume in the water column for which void fractions at higher air detrainment rates were corrected.

2.4. Physical Properties of mPMA

Air was sampled from the generator's headspace at 5.5 L min^{-1} through a downward facing 1.59 cm ID port. During most intervals, sample air was drawn from the port through a custom-fabricated diffusion dryer with a 1.91 cm ID stainless steel mesh tube surrounded by silica gel. A custom-fabricated stainless steel splitter (1.59 cm ID × 3.8 cm long tube with a 0.476 cm ID sidearm sampling port) connected the outlet of the dryer to the inlet of an aerodynamic particle sizer (APS, TSI Model 3321), which was positioned directly below the sampling port on the generator. Sample plus sheath air was drawn at 5 L min^{-1} into the APS. Air was subsampled through the sidearm port at 0.5 L min^{-1} and transferred through a 0.476 cm ID × 64 cm long stainless steel tube to a Scanning Electrical Mobility Spectrometer (SEMS, Brechtel Manufacturing, Inc.). The SEMS's sheath air was drawn separately from room air.

The in-line dryer dehydrated mPMA to a RH of approximately 25% (hereafter referred to as "dry"). Unless otherwise noted, all number and mass size distributions reported herein correspond to dry aerosol. As described in more detail below, for some characterization experiments, the dryer was removed and replaced with a 1.59 cm ID stainless steel tube.

The SEMS quantified size-resolved mobility diameters of mPMA between 0.010 and 1.0 μm. The APS measured size-resolved aerodynamic diameters that, based on an assumed density of 2.12 g cm^{-3} (Quinn & Coffman, 1998), were converted to mobility diameters between 0.37 and 15 μm. Assuming further that all particles were spherical (no shape corrections were applied), mobility diameters were assumed to be

approximately equal to geometric diameters. The 56 size bins less than 0.62 μm geometric diameter measured with the SEMS were merged with the 43 size bins greater than 0.62 μm geometric diameter measured with the APS. Distributions were not integrated or smoothed across the merge point. The geometric mean diameter (GMD) for each size bin was calculated as the square root of the product of the upper and lower limits for the corresponding diameter range. Integration times for both instruments were 5 min during WACS and 5 and 6 min for the SEMS and APS, respectively, during CalNex. These instruments yield representative size distributions of marine aerosol (Reid et al., 2006).

The production efficiency of mPMA number per unit volume of air detrained (PE_{num}, in units of L^{-1}) was calculated directly from the measured number size distribution (L^{-1}) multiplied by the flow rate of sweep plus bubble air through the generator (L min^{-1}) divided by the corresponding rate at which bubble air detrained across the air-water interface (L min^{-1}). The production efficiency of mPMA mass per unit volume of air detrained (PE_{mass}, in units of μg L^{-1}) was calculated based on the measured volume size distribution, a density of 2.14 g cm^{-1} for particles greater than 1 μm dry diameter (which were dominated by inorganic sea salt), a density of 1.84 g cm^{-1} for particles less than 1 μm diameter (which were a mixture of inorganic sea salt and OM), the flow rate of air through the generator, and the corresponding air detrainment rate across the interface (Long, Keene, Kieber, et al., 2014).

2.5. Chemical Properties of mPMA

mPMA for chemical characterization was not dried prior to sampling. Size-resolved mPMA was sampled through two downward facing 2.22 cm ID ports at 30 L min^{-1} over nominal 20 h periods with nonrotating Multi-Orifice Uniform Deposit Impactors (Marple et al., 1991). The 50% aerodynamic diameter cut sizes were 0.18, 0.32, 0.56, 1.00, 1.8, 3.2, 5.6, 10.0, and 18 μm yielding GMDs for the 10 size fractions of 0.13, 0.24, 0.42, 0.75, 1.34, 2.40, 4.23, 7.48, 13.4, and 25.5 μm. Approximate GMDs for the smallest and largest size fractions are based on an assumed lognormal distribution with the lower and upper limits, respectively, for the corresponding cut sizes defined by the same log bin widths (e.g., for the smallest size bin, GMD = $0.18/2^{0.5}$). Impactors for characterization of ionic constituents during CalNex were configured with 47 mm polycarbonate substrates (Whatman 111107) and 37 mm diameter quartz backup filters. Impactors for characterization of OC during CalNex and impactors for analysis of both ionic constituents and OC during WACS were configured with precombusted 47 mm diameter aluminum substrates and 37 mm diameter quartz backup filter. During both campaigns, mPMA was also sampled in bulk at 30 L min^{-1} on precombusted 47 mm quartz filters.

After recovery, size-resolved samples for analysis of major ions were transferred to precleaned 10 mL high-density polyethylene tubes, stored frozen, subsequently extracted in 5 mL deionized water (DIW), and analyzed by high-performance ion chromatography (IC) at the University of Virginia (UVA). During CalNex, entire bulk filter samples were extracted in 8 mL DIW and analyzed for major ions by IC at UVA. During WACS, bulk samples for analysis at UVA were cut in half prior to extraction. One half of each sample was extracted in 5 mL DIW and analyzed for major ions as described above. The other half was analyzed for total organic carbon (OC_{tot}) with a Sunset Laboratory Thermal/Optical Analyzer (Birch & Cary, 1996). Size-segregated and bulk samples for analysis of water-extractable OC (OC_{we}) were transferred to precombusted 10 mL Pyrex centrifuge tubes, extracted immediately after recovery in 5 mL DIW, stored frozen, and analyzed in triplicate at the State University of New York using a Shimadzu Model TOC-V CSH carbon analyzer. Detection limits for ionic analytes and OC_{we} reported herein were estimated following Keene et al. (1989), and measurement precisions were estimated based on replicate analyses. Data quality metrics are summarized in Table S1 in the supporting information.

A linear regression of OC_{we} versus OC_{tot} measured in a subset of paired bulk samples that were collected in parallel during WACS yielded a significant linear relationship with a slope of 0.62, an intercept of −27.1 nmol C m^{-3}, and a r^2 of 0.999. OC_{tot} concentrations ranged from 62 to 244 nmol C m^{-3}. This relationship indicates that OC_{tot} was not recovered quantitatively by the extraction procedure. Consequently, OC_{we} data reported herein correspond to lower limits for total OC. Organic enrichment factors relative to seawater ($EF(OC_{we})$) were calculated as the ratio of OC_{we} versus Na^+ (for WACS) or Mg^{2+} (for CalNex) measured in mPMA samples divided by the corresponding ratio measured in the bulk seawater from which the aerosol was produced. Because relative analytical precision for Na^+ versus Mg^{2+} differed between the two

Table 1
Times, Locations, Meteorological Conditions, and Seawater Characteristics

	WACS-S1[a]	WACS-S2[a]	CalNex[b]
Start characterization, local time	20 August 2012, 0820	24 August 2012, 0939	15 May 2010, 1420
Stop characterization, local time	23 August 2012, 1001	26 August 2012, 1650	7 June 2010, 1217
Start latitude/longitude	41.88°N/67.40°W	36.79°N/65.34°W	33.90°N/118.49°W
Stop latitude/longitude	41.70°N/67.14°W	36.20°N/64.37°W	37.77°N/122.63°W
Wind speed[c] (m s^{-1})	2.6 ± 1.5	5.2 ± 2.0	4.7 ± 3.1
Peak daily insolation[c] (W m^{-2})	798 ± 108	754 ± 369	999 ± 150
Sea surface temperature[c] (°C)	18.1 ± 0.2	28.5 ± 0.2	14.5 ± 1.4
Salinity[c] (ppt)	32.5 ± 0.02	35.9 ± 0.1	32.9 ± 1.0
Chl *a*[d] (μg L^{-1})	6.9 (2.7–13.9)	<0.05 (<0.05–0.24)	2.1 (0.02–29.4)
Seawater DOC[c] (μ*M*)	88.2 ± 1.7 (*N* = 4)	73.4 ± 3.6 (*N* = 4)	62.2 ± 3.9 (*N* = 5)
Near-surface bubble diameter (Coarse frit)[d], (mm)	0.44 (0.23–0.89) (*N* = 219)[e]	0.47 (0.28–1.41) (*N* = 250)[f]	0.37 (0.32–0.48) (*N* = 50)[g]
Near-surface bubble diameter (fine frits)[d], (mm)	0.35 (0.23–0.54) (*N* = 195)[h]	0.33 (0.24–0.46) (*N* = 112)[i]	0.35 (0.18–0.50) (*N* = 198)[j]
Bubble air residence time (coarse frit)[k] (s)	2.9	2.5	3.8
Bubble air residence time (fine frits)[k] (s)	9.5	8.1	11.8

Note. *N* designates number of individual measurements.
[a]Excludes data for ferry cruises to and from stations. [b]Excludes data for in-shore waters (Los Angeles Harbor, San Francisco Bay, and Sacramento River). [c]Mean ± standard deviation. [d]Median (range). [e]Measured on 22 and 23 August 2012 during transition between daytime and late night. [f]Measured on 24 and 26 August 2012 during transition between late night and daytime. [g]Measured on 31 May 2010 during daytime. [h]Measured on 20 and 22 August 2012 during daytime. [i]Measured on 24 August 2012 during transition between late night and daytime. [j]Measured on 29 May and 1 June 2010 during daytime. [k]Based on slopes of void fractions versus air detrainment rates (Figure 1).

campaigns, corresponding EF(OC_{we})s were based on the reference species with the greatest relative precision (e.g., Keene et al., 1986).

3. Results and Discussion

Sampling times, locations, and environmental characteristics for WACS-S1, WACS-S2, and CalNex are summarized in Table 1. All dates and times reported herein correspond to local times. Both campaigns were conducted during boreal spring (CalNex) or summer (WACS) and under conditions of relatively low wind speeds and sea states. However, differences in ship operations during the two campaigns constrain direct comparison of results. During WACS, the ship occupied two oceanographic stations for 2 to 3 days each in (1) biologically productive waters on Georges Bank and (2) the oligotrophic Sargasso Sea. The median Chl *a* concentrations at WACS-S1 and WACS-S2 were 6.9 and less than 0.05 μg L^{-1}, respectively. All measurements for WACS reported herein correspond to mPMA produced from these discrete seawater types. Consequently, spatial variability in water type during sampling at each WACS station was a relatively minor source of variability in results. In contrast, during CalNex most characteristics of the system were measured when the ship was in transit along the California coast through distinct water types that varied chemically and biologically (Table 1) (Long, Keene, Kieber, et al., 2014). For example, Chl *a* concentrations during CalNex ranged from 0.02 to 29.4 μg L^{-1}. Consequently, spatial variability in seawater properties contributed substantially to overall variability in the CalNex results. In addition to differential influences associated with ship operations, mPMA emissions from biologically productive waters (WACS-S1 and CalNex) varied systematically over diel cycles (Long, Keene, Kieber, et al., 2014). Consequently, spatial variability in seawater types during CalNex and temporal variability in mPMA production both at WACS-S1 and during CalNex constrain resolution in evaluating characteristics of the system that were measured at different times. Therefore, caution is warranted when interpreting results for WACS-S1 and CalNex that are not coincident in time. To provide context for comparing data that were generated at different times, we report results using the same time convention employed by Long, Keene, Kieber, et al. (2014). "Daytime" is defined as 4 h following sunrise through 2 h following sunset, "nighttime" is defined as the 6 h preceding sunrise, "transitions" are periods that fall between those specified as daytime and nighttime, and "mixtures" include periods that bridge two or more of the three specified periods.

3.1. Seawater Characteristics That Influence Bubble Plume Dynamics and Bubble Bursting

3.1.1. Salinity and Temperature

Over naturally occurring ranges in seawater, temperature and salinity impact bubble interactions within plumes through modulation of seawater density, surface tension, and to a lesser extent viscosity (e.g., see

Burns & Zhang, 2001; Holcomb & Zollweg, 1992; Sadhal et al., 1997). Available evidence from other studies (e.g., Salter et al., 2014, 2015) suggests that temperature-dependent variability in bubble plume dynamics and associated mPMA production over the range in seawater temperatures during WACS and CalNex (Table 1) was a relatively minor (less than ~10%) source of variability in results. Similarly, the narrow range of surface-water salinities (Table 1) suggests that variability in salinity was a negligible source of variability in results (Lewis & Schwartz, 2004). As discussed further in section 3.2, the presence of surfactants significantly dampens the impact of both temperature and salinity on bubble plumes generated by porous media (Burns & Zhang, 2001). Because previous investigations of temperature and salinity focused primarily on water devoid of or at unknown concentrations of surfactants, the reported influences may not be representative of those for natural, surfactant-rich seawater.

3.1.2. Surfactant DOC and Bubble Surface Tension

Although median Chl *a* concentrations, an indicator of algal biomass, during the measurement periods evaluated herein varied over a factor of greater than 10^2, the corresponding DOC concentrations fell within a relatively narrow range (Table 1). DOC in the surface ocean is composed of a wide variety of compounds including short-lived, labile species that are readily metabolized on time scales of less than a day; semilabile and semirecalcitrant species with average lifetimes of 1.5 and 20 years, respectively; and recalcitrant DOC (RDOC) with an average lifetime of 16,000 years (Hansell, 2013). RDOC accounts for about 95% of all DOC in the global ocean and, typically, comprises greater than 50% to almost 100% of DOC in surface waters. Because relatively long-lived (>1 year to millennia) compounds dominate DOC in the surface ocean (Hansell, 2013), DOC concentrations are rather insensitive to variability in recent biological activity as indicated by Chl *a*, consistent with results reported in Table 1.

Measurements of dynamic bubble surface tension at both WACS-S1 and WACS-S2 ranged from 0.4 to 1.2 mN m^{-1} below that of artificial seawater at equivalent temperature and salinity but with no organics and thus no surface-active compounds (Long, Keene, Kieber, et al., 2014). These and related results from associated manipulation experiments indicate that DOC in both biologically productive and oligotrophic surface water includes surfactant OM that coats bubble surfaces. Time series measurements and manipulation experiments also revealed that distinct reservoirs of short-lived surfactants modulate bubble characteristics leading to enhanced mPMA production during daytime relative to nighttime in biologically productive waters at WACS-S1 and during CalNex (Long, Keene, Kieber, et al., 2014). Dynamic surface tension depressions measured in North Atlantic Deep Water sampled at a depth of 2,505 m at WACS-S2 (1.1 ± 0.2 mN m^{-1}) were also similar to those in surface waters (Kieber et al., 2016). This behavior indicates that labile DOC and RDOC (and presumably semilabile and semirecalcitrant DOC) in surface seawater include surfactant OM that rapidly (seconds) adsorbs onto bubble surfaces and produces organic films. These films stabilize bubbles against coalescence (e.g., Deane & Stokes, 2002) and thereby modulate bubble size, rise velocity, bursting behavior, and bubble surface area delivered to the air-water interface per unit air detrained. Results also reveal that for a given set of conditions, surface tension evolved temporally in response to the diffusion of surfactants to and competition among surfactants for available bubble surface area. The temporal evolution of surface tension varies as functions of the relative concentrations, composition, and associated diffusion rates and surface affinities of the surfactant compounds present (Adamson & Gast, 1990). However, due to method constraints at sea, most measurements of dynamic surface tension were limited to surface ages less than 2 s, and thus, results could not be interpreted directly in terms of the corresponding plume characteristics or mPMA production via the bursting of the relatively longer-lived bubbles within the generator (Table 1).

3.2. Bubble Plume Dynamics

Results presented in the preceding section suggest that variability in organic surfactants associated with different water types drives corresponding variability in bubble plume dynamics. Steady state void fractions produced with fine frits (0.015 to 0.020 L_{air} L_{sw}^{-1}) at typical air detrainment rates employed for this study (2.0 to 2.5 L m^{-2} s^{-1}, Figure 1) overlapped the range of those measured at 30 cm depth during the quiescent phase of bubble plumes produced by ambient wind waves in coastal waters off Southern California, USA, during winter (0.007 to 0.065 L_{air} L_{sw}^{-1}) (Deane & Stokes, 2002). Void fractions produced with the coarse frit (0.003 to 0.005 L_{air} L_{sw}^{-1}) were near the lower limit of reported values. For each set of conditions, the void fraction was linearly correlated with air detrainment rate. However, the corresponding slopes varied

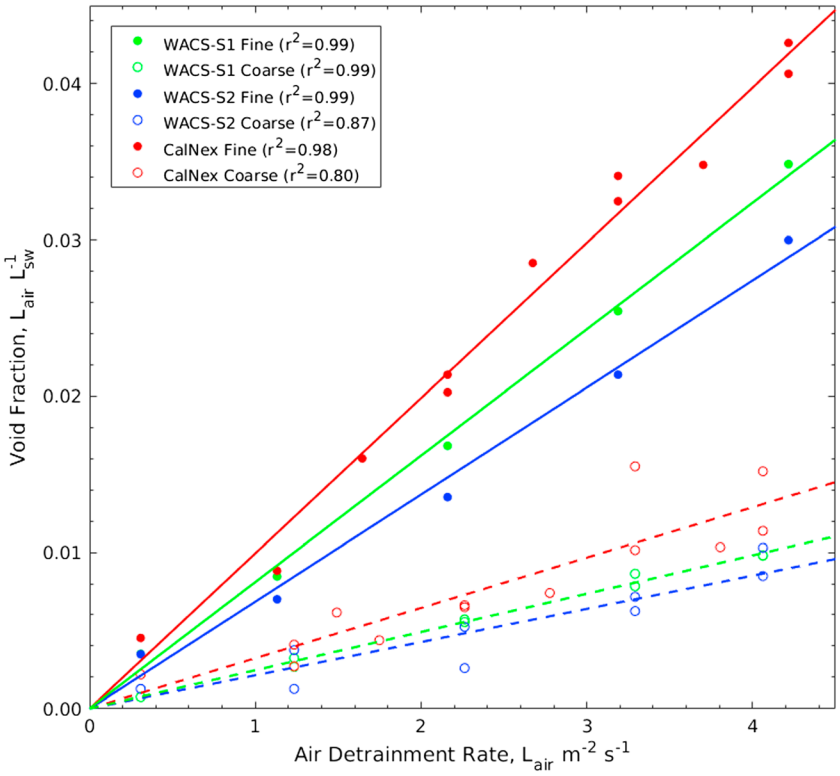

Figure 1. Steady state bubble plume void fraction versus air detrainment rate generated with the coarse frit (open symbols and dashed lines) and fine frits (solid symbols and solid lines) at WACS-S1 (in green on 20 August 2012 from 0820 to 0905), at WACS-S2 (in blue on 24 August 2012 from 1830 to 2110), and during CalNex (in red on 15 May 2010 from 1421 to 1656). Lines depict standard linear regressions; corresponding r^2 values appear in the legend. Dates and times reported above and in subsequent figures and captions correspond to local times.

systematically as functions of both frit porosity and seawater type (Figure 1). For each seawater type, the steady state void fraction for bubbles produced by fine frits at a given air detrainment rate was about 3 times greater on average than that produced by the coarse frit. We infer that these differences were driven primarily by differences in the initial bubble sizes produced by the two frit porosities in each seawater type and corresponding differences in bubble lifetimes in the column. Although the configuration of the generator did not allow measurements of the initial bubble size distributions, sizes of aged bubbles near the air-water interface were quantified (Table 1).

Residence times of bubble air within the water column (Table 1) were calculated from the regression slopes of void fraction versus air detrainment rate depicted in Figure 1. Relative to fine frits, the coarse frit produced larger bubbles with faster rise velocities (approximately 28 cm s^{-1} versus 9 cm s^{-1}) and thus shorter lifetimes in the water column, which sustained smaller steady state void fractions. *T* tests of paired slopes for void fractions versus air detrainment rates produced by fine frits in distinct water types differed significantly at α of 0.05. Although the corresponding trend in slopes for the coarse frit was similar to that for fine frits (i.e., WACS-S2 $<$ WACS-S1 $<$ CalNex), the differences among those slopes were statistically indistinguishable. Random variability associated with motion of the ship coupled with the relatively small numbers of observations limited statistical resolution in evaluating the significance of what we suspect is a representative trend in the dynamics of plumes produced by the coarse frit in different seawater types. Median sizes and distributions of near-surface bubbles produced by fine frits were statistically indistinguishable. Because the final bubble sizes produced by fine frits in different seawater types were similar, we infer that variability among void fractions may have been driven by differences in the initial bubble sizes (and associated rise velocities) coupled with the subsequent evolution toward similar bubble size near the air-water interface.

Bubble size in a plume generated by sintered-frit aeration is affected by many system parameters including frit porosity, fluid and gas temperature and density, hydrostatic pressure, air flow rate (analogous to inlet

Table 2
Seawater DOC Concentration ± Standard Deviation in μM at Inlet and Outlet of Generator

Date, time (local)	Frit porosity	Inlet	Outlet
WACS-S1			
22 Aug 2012, 0930[a]	Fine	85.9 ± 0.4	87.0 ± 0.8
22 Aug 2012, 1637[b]	Coarse	90.6 ± 2.4	90.2 ± 2.1
23 Aug 2012, 0555[c]	Coarse	88.8 ± 2.2	91.9 ± 2.0
Average ± SD		88.4 ± 1.9	89.7 ± 2.0
WACS-S2			
24 Aug 2012, 0817[a,d]	Fine	74.6 ± 2.1	52.3 ± 5.1
25 Aug 2012, 1023[a]	Fine	74.0 ± 1.9	56.2 ± 1.5
26 Aug 2012, 0828[a]	Coarse	74.5 ± 0.5	45.6 ± 0.8
Average ± SD		74.3 ± 0.3	51.4 ± 4.4

[a]Transition between late night and daytime. [b]Daytime. [c]Late night. [d]Sampled in the Sargasso Sea but approximately 1 h before the ship arrived at station 2.

pressure), and surface tension. However, the presence of surfactants substantially diminishes the impact of other system parameters on the resulting bubble plume characteristics (Burns & Zhang, 2001). Evidence from other studies suggests that bubbles smaller than about 2 mm diameter (which includes virtually all of those produced within the generator) are stabilized by natural surfactants in seawater, and consequently, do not fragment (or presumably coalesce) (e.g., Deane & Stokes, 2002). As noted above, however, bubble surface tension is not static but evolves over time in response to the concentrations, speciation, and associated surface affinities of the dissolved OM that competes for available surface area in different seawater types (Long, Keene, Kieber, et al., 2014). Consequently, the initial bubble size (and associated buoyancy and rise velocity) may evolve via simple expansion or contraction in response to evolving bubble surface tension. Presumably, the initial bubble sizes produced by frits also varied among seawater types as a function of surface tension (Burns & Zhang, 2001).

Similarly, differences in bubble size reflect corresponding differences in the age of bubble surfaces and associated surface tension. Consequently, the dynamics of plumes produced by different frit sizes in a given seawater type can be interpreted as two points along a time series of surface evolution in response to the same reservoir of surfactants. For example, relative (but insignificant) differences among slopes for void faction versus air detrainment rate for plumes composed of shorter-lived bubbles produced by the coarse frit in different seawater types are similar to those for plumes composed by longer-lived bubbles produced by fine frits in different seawater types (WACS-S2 < WACS-S1 < CalNex, Figure 1). These results suggest that despite differences in bubble surfaces exposed to each seawater type and associated surface tensions at different ages, bubble properties in all seawater types evolved in similar relative directions. Although the primary mechanism(s) responsible for the variability in void fractions among different seawater types cannot be resolved unequivocally, our observations clearly indicate that such variability exists and presumably relates in part to variability in concentrations and/or speciation of the dominant surface-active OM present in these different waters. By extension, these results suggest that interactions between surfactant OM and bubble plume surfaces may also influence DOC concentrations and speciation in surface seawater.

3.3. Processing of Surfactant DOC by Bubble Plumes

The aerosol generator is a closed system. The only pathways by which OM originally present in feed seawater could be removed are via (1) incorporation into mPMA and (2) overflow to the seawater exhaust drain. Less than 0.01% of DOC flowing through the generator was recovered as OC_{we} associated with mPMA (Long, Keene, Kieber, et al., 2014), and consequently, virtually all OM that entered the generator through the inlet left the generator via the seawater exhaust line. DOC concentrations at the inlet and at the outlet did not vary significantly as functions of frit size or time of day (daytime versus transition) at either WACS-S1 or WACS-S2 (Table 2). However, at WACS-S2, DOC concentrations at the exhaust were significantly lower than those at the inlet by an average of 31%. These results indicate that a significant fraction of DOC in oligotrophic seawater at WACS-S2 was removed from solution via bubble processing. Samples for analysis of DOC were drawn from the generator through 0.2 μm Whatman POLYCAP 75 AS cartridges. We hypothesize that bubble processing converted a significant fraction of DOC originally present at WACS-S2 to particulate OM, perhaps as gels (e.g., Barber, 1966), of sufficient size and lifetime against redissolution (minutes) to be removed by the POLYCAP cartridges.

In contrast, DOC concentrations measured at the generator's inlet and exhaust at WACS-S1 were statistically indistinguishable indicating that bubble processing had minimal influence on bulk DOC concentrations at this station. If interactions of OM with bubble surfaces produced particulate OM at WACS-S1, these results suggest that the particles were either too small or too short lived against redissolution to be removed by the POLYCAP particle filters or they were present at sufficiently low abundance for detection via changes in DOC. Evidence reported by Long, Keene, Kieber, et al. (2014) supports the hypothesis that surfactants in oligotrophic seawater at WACS-S2 were associated with a spatially uniform background reservoir of DOC,

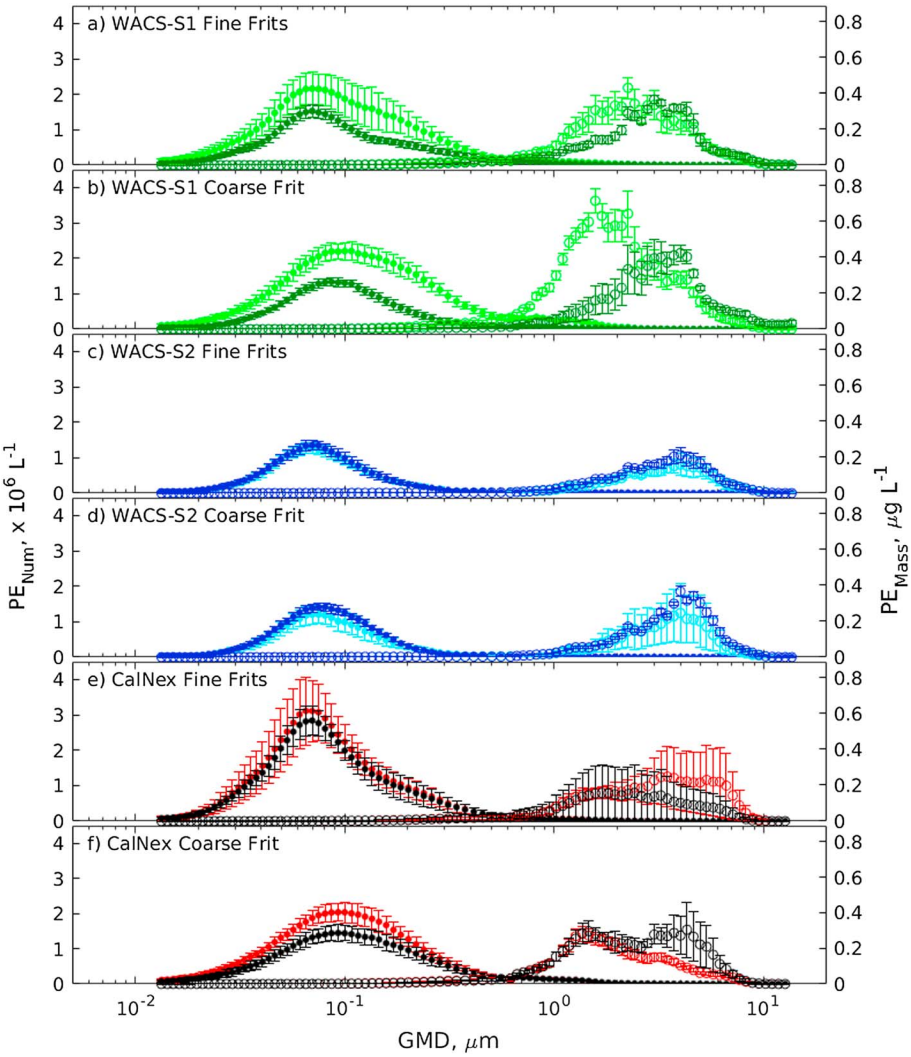

Figure 2. Average size-resolved PE_{num} (solid symbols, *Y* axis) and PE_{mass} (open symbols, second *Y* axis) during daytime (lighter colors) and nighttime (darker colors) at WACS-S1 (green) using (a) fine frits (Ns = 89 for daytime and 107 for nighttime) and (b) the coarse frit (Ns = 72 for daytime and 68 for nighttime); at WACS-S2 (blue) using (c) fine frits (Ns = 75 for daytime and 75 for nighttime) and (d) the coarse frit (Ns = 53 for daytime and 59 for nighttime); and during CalNex using (e) fine frits (Ns for the SEMS and APS = 162 and 142, respectively, for daytime and 205 and 182, respectively, for nighttime); and (f) the coarse frit (Ns for the SEMS and APS = 176 and 94, respectively, for daytime and 134 and 114, respectively, for nighttime). Ns denote numbers of scans. Errors bars depict ±1 standard deviation. During WACS, air detrainment rates for fine and coarse frits were 2.2 and 2.3 L m^{-2} s^{-1}, respectively. During CalNex, detrainment rates for fine frits ranged from 0.9 to 2.2 L m^{-2} s^{-1} and for the coarse frit ranged from 1.0 to 1.8 L m^{-2} s^{-1}.

whereas a distinct reservoir of OM containing surfactants with relatively stronger surface affinities was present in biologically productive waters (WACS-S1 and CalNex) during daytime. We infer that the relatively small reservoir of surfactants that originated from biological and/or photochemical sources on diel scales at WACS-S1 effectively out-competed the background surfactants for bubble surfaces, thereby preventing the formation of larger, longer-lived, and/or more abundant organic particulates via interactions of background surfactants with bubble surfaces.

3.4. Primary Factors That Influence PE_{num} and PE_{mass}

The environmental and operational factors that modulate bubble plume dynamics discussed above also impact the corresponding production of mPMA when bubbles burst at the air-water interface. These and other factors are evaluated below.

Table 3
Summary Statistics for Total PE_{num} and PE_{mass}

Characteristic	WACS-S1 Fine frits	WACS-S1 Coarse frit	WACS-S2 Fine frits	WACS-S2 Coarse frit	CalNex Fine frits	CalNex Coarse frit
			PE_{num}			
Total daytime[a] ($\times 10^6$ L^{-1})	55.4 ± 13.1	61.1 ± 5.8	23.0 ± 0.9	22.4 ± 5.0	63.1 ± 15.9	53.0 ± 4.6
Total nighttime[a] ($\times 10^6$ L^{-1})	32.4 ± 1.7	27.7 ± 2.4	24.4 ± 1.0	26.2 ± 0.8	56.9 ± 6.3	37.3 ± 7.8
Peak GMD daytime (μm)	0.070	0.108	0.065	0.075	0.070	0.093
Peak GMD nighttime (μm)	0.070	0.086	0.070	0.081	0.070	0.093
			PE_{mass}			
Total daytime[a] (μg L^{-1})	7.2 ± 0.7	11.8 ± 1.2	2.7 ± 0.6	3.6 ± 2.2	5.8 ± 2.8	5.1 ± 0.5
Total nighttime[a] (μg L^{-1})	5.8 ± 0.3	7.0 ± 1.6	3.4 ± 0.3	4.7 ± 0.3	3.7 ± 0.6	6.8 ± 1.8
Peak GMD daytime (μm)	2.25	1.57	4.00	4.00	3.47	1.36
Peak GMD nighttime (μm)	3.00	4.00	4.00	4.00	2.42	1.46

Note. Based on mean size distributions depicted in Figure 2. See Figure 2 caption and associated text for additional details.
[a]Mean ± standard deviation.

3.4.1. Frit Porosity, Seawater Composition, and Time of Day

Size-resolved PE_{num} and PE_{mass} were measured continuously under invariant sets of operating conditions during the long (nominal 20 h) cascade impactor sampling intervals. Subsets of values for sampling intervals during which mPMA was produced using fine-porosity frits and using the coarse-porosity frit were averaged over discrete daytime and nighttime periods at the two WACS stations and during CalNex (Figure 2). These plots depict the actual measured PEs per unit air detrained for each size bin rather than PEs that have been normalized based on the corresponding widths of size bins (Dp). The narrow ranges in log Dp for the SEMS (0.028 to 0.041 μm) and the APS (0.027 to 0.031 μm) indicate that the relative shapes of PE_{num} and PE_{mass} distributions depicted in Figure 2 are very similar to those of the corresponding normalized distributions for $dPE_{num}/dlogDp$ and $dPE_{mass}/dlogDp$, respectively, as illustrated by the example shown in Figure S1. The slight deviations between relative shapes of the plotted versus underlying distributions do not impact interpretation of results. We employ this plotting convention to facilitate direct comparisons with previously reported results based on the same approach (Kieber et al., 2016; Long, Keene, Kieber, et al., 2014) and with the corresponding size-resolved chemical data, which are not normalized herein or typically elsewhere based on widths of size bins. The total PE summed over each size distribution depicted in Figure 2 and the corresponding GMD for the mPMA size fraction with the peak PE for each distribution are summarized in Table 3.

The generator was operated in the same configurations at the two WACS stations, and consequently, for a given configuration, differences between PEs at these stations were driven primarily by differences in seawater characteristics. In contrast, during CalNex, PEs were measured over air detrainment rates ranging from 0.9 to 2.2 L m^{-2} s^{-1}, which as discussed in more detail below, contributed to variability in PE, particularly in PE_{mass}. In addition, spatial heterogeneity in seawater characteristics during CalNex including potential influences of surfactant OM originating from Ekman-induced coastal upwelling, benthic biota (e.g., macroalgae), and nonmarine sources (e.g., terrestrial runoff and hydrocarbon seeps from the sea floor) contributed to variability in PEs. Consequently, PEs during CalNex were generally more variable relative to those during WACS (Table 3).

Size-resolved PE_{num} values for both coarse and fine frits were significantly greater during daytime relative to nighttime at the biologically productive WACS-S1 whereas diel variability at the oligotrophic WACS-S2 was insignificant (Figure 2 and Table 3) as reported previously (Long, Keene, Kieber, et al., 2014). In addition, PE_{num} values during the night were similar at both WACS stations. PE_{num} values during CalNex were also higher during daytime relative to nighttime although diel differences for the fine frits were not significant. In all cases, the peak in PE_{num} values for the coarse frit was associated with larger GMDs relative to that for fine frits. In addition, relative differences between the peak GMDs for PE_{num} associated with coarse versus fine frits were greater for biologically productive waters (WACS-S1 and CalNex) than those for the oligotrophic WACS-S2 (Table 3).

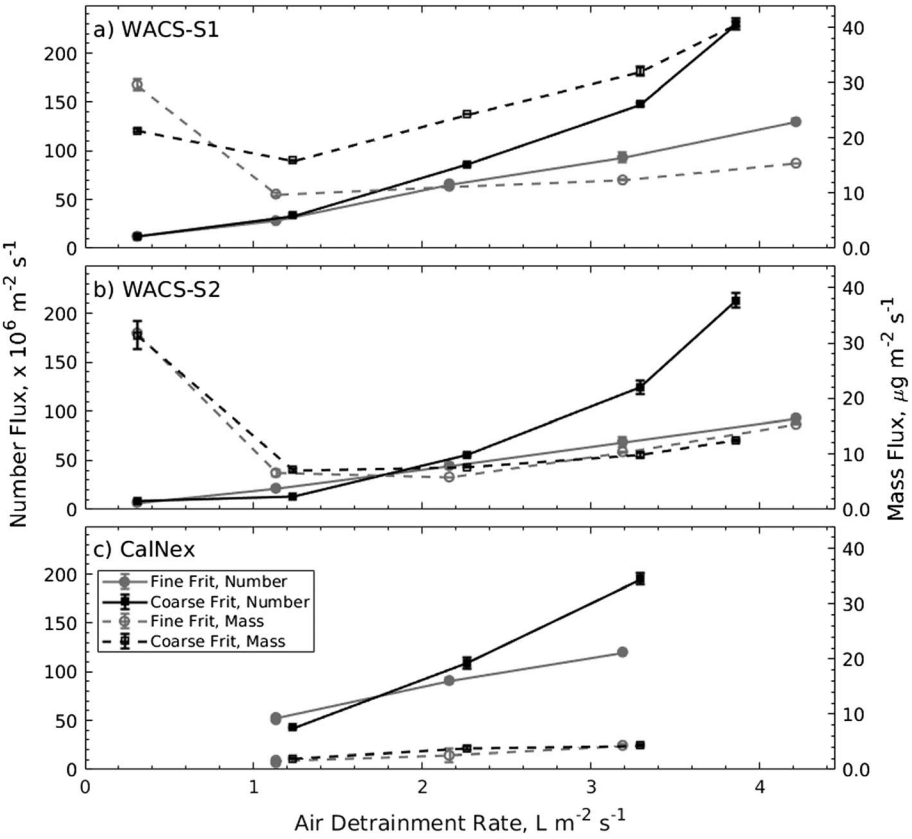

Figure 3. Total production flux of mPMA number (solid symbols and connecting lines, *Y* axis) and mass (open symbols and dashed connecting lines, second *Y* axis) versus air detrainment rate using fine (gray) and coarse (black) frits (a) at WACS-S1 on 20 August 2012 between 1006 and 1318, (b) at WACS-S2 on 24 August 2012 between 0939 and 1320, and (c) during CalNex on 1 June 2010 between 1006 and 2009. One full size-resolved flux distribution generated with fine frits at an air detrainment rate of 2.16 L m^{-2} s^{-1} was measured at WACS-S1. All other total fluxes correspond to the average for two (during WACS) or three (during CalNex) size-resolved distributions measured consecutively. Error bars depict range for WACS and ±1 standard deviation for CalNex.

Size-resolved and total PE_{mass} values for both coarse and fine frits at WACS-S1 were greater and shifted toward smaller GMDs during daytime relative to nighttime (Figures 2a and 2b and Table 3). In contrast, at WACS-S2, PE_{mass} values for coarse and fine frits exhibited similar size distributions during the daytime and nighttime. PE_{mass} values for CalNex were more variable with no consistent day-night trends observed. Although marine-derived OM accounts for minor to negligible fractions of mPMA mass (discussed in more detail below), the results for WACS-S1 indicate that surfactant OM in the surface ocean significantly modulates the size-resolved production of mPMA mass from the surface ocean.

Systematic diel variability was evident in PE_{num} and PE_{mass} at WACS-S1 and over some periods during CalNex but not at WACS-S2. Available evidence supports the hypothesis posed by Long, Keene, Kieber, et al. (2014) that these day-night differences for biologically productive waters reflect influences of dominant but short-lived surfactant pools that are produced via biological and/or photochemical pathways in the near-surface ocean during daytime. At WACS-S1 and over some relatively less variable periods during CalNex, these daytime pools were rapidly depleted following sunset revealing the influence of a larger background reservoir of surfactants that modulated mPMA generation from biologically productive waters at night and from oligotrophic waters. Surfactants associated with RDOC likely contribute to this background reservoir (Kieber et al., 2016).

3.4.2. Air Detrainment Rate and Surface Bubble Rafts

As noted previously, PE_{num} values during daytime varied among different seawater types (Table 3). Standard linear regressions indicate that the total mPMA number production flux generated with fine frits from each

seawater type during daytime was significantly correlated with air detrainment rate (r^2 for WACS-S1 = 0.994, r^2 for WACS-S2 = 0.998, and r^2 for CalNex = 0.994; Figure 3). Significant linear correlations between number production fluxes generated with fine frits versus air detrainment rates were also observed during a previous deployment of the generator at Bermuda (Keene et al., 2007). At air detrainment rates less than about 2 L m^{-2} s^{-1}, number production fluxes generated with the coarse frit in all seawater types during daytime were similar to those generated with fine frits but, at higher detrainment rates, those generated with the coarse frit were disproportionately greater and the magnitude of divergence increased with increasing detrainment rate (Figure 3). Consequently, PE_{num} for the coarse frit varied as a function of air detrainment rate. Presumably, the marked divergence at higher detrainment rates was driven in part by physical processes involving the relatively greater energy dissipated at the air-water interface by the larger sizes and faster rise velocities of bubbles produced by the coarse frit. However, the mechanism responsible for the curvilinear relationship between mPMA production versus air detrainment rate for the coarse frit cannot be resolved unequivocally based on available data.

Relationships between mass production fluxes of mPMA versus air detrainment rates at the two WACS stations during daytime were highly nonlinear and counterintuitive (Figures 3a and 3b). For both frit porosities at WACS-S2 and for fine frits at WACS-S1, the lowest detrainment rates produced the maximum mass fluxes. The total mPMA mass produced by the coarse frit at WACS-S1 was also greater at the lowest detrainment rate relative to the next higher rate. The number and mass production fluxes of size-resolved mPMA produced by fine frits as a function of air detrainment rate at WACS-S1 (Figure 4) indicate that mass production was dominated by a proportionately very small number of relatively large particles. Clearly, physical processes other than air detrainment alone are important in modulating mPMA mass production fluxes.

We hypothesize that the above relationships reflect influences of bubble-bubble and bubble-surface interactions within bubble rafts (the physical ramifications of breaking-wave whitecaps) on the injection of larger droplets that dominate production of mPMA mass. Visual inspection indicates that low air detrainment rates sustain surface rafts that are both discontinuous across the air-water interface and relatively thin, whereas higher detainment rates sustain rafts that are more continuous across the interface and relatively thick. Bubbles that burst within raft structures do not produce the classic cavities at the air-water interface that inject jet droplets. In these cases, we infer that energy is dissipated primarily by interactions with and displacement of surrounding bubbles in the raft. Bubbles that burst at the bottom of raft structures produce cavities at the interface, but the injection of jet droplets may be attenuated by overlying bubble structures. Based on the above discussion, we hypothesize that bursting bubbles uninfluenced by surface rafts emit jet droplets and associated mPMA mass at higher efficiency per unit air detrained relative to those associated with rafts. If this hypothesis is correct, the mass production efficiency (i.e., PMA mass flux per unit air detrained or per unit energy dissipated) by breaking waves may be substantially greater at lower wind velocities and associated whitecap coverage relative to higher velocities and with smaller shorter-lived breaking events common under all wind regimes. Similarly, for a given sea state, PMA mass fluxes may be dominated by the relatively lower volumes of plume air that detrain as individual bubbles around the perimeters of fully developed whitecaps or during the dissipation phases of whitecaps relative to the larger volumes of air that detrain through whitecaps. It was evident from visual inspection that the dynamics of raft structures (thickness, bubble size, and lifetime) also varied substantially in response to seawater type. Although poorly characterized, we infer from the above that in addition to the other effects discussed previously, surfactant OM influenced the production of mPMA mass via modulation of raft structures. To our knowledge, the potentially important influences of spatial and temporal variability in surface bubble rafts as functions of sea state and seawater composition suggested by our results have not been considered explicitly in any parameterizations of PMA production reported to date. We return to this issue in section 4.2.

In this regard, we note that sea state influences the lifetime of surface bubble rafts within the generator when deployed on a ship at sea. Under calm seas, the raft drained evenly over the circumference of the air-water interface whereas, under rough seas, the ship's motion resulted in more variable drainage and redevelopment of raft structures. Although not controllable or characterized explicitly, variability in sea state during the two campaigns clearly contributed to variability in raft dynamics within the generator and, we speculate, corresponding variability in PE_{mass} under otherwise identical operating conditions.

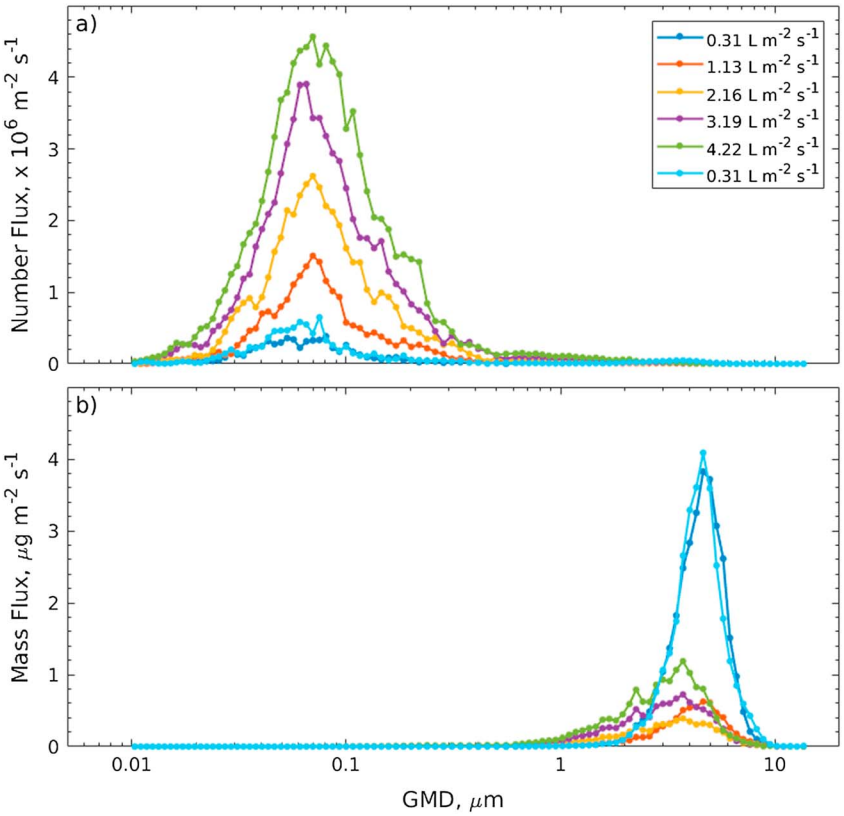

Figure 4. Size-resolved production flux of mPMA (a) number and (b) mass generated with fine frits over a range in air detrainment rate at WACS-S2 on 24 August 2012 between 0939 and 1134. Each size-resolved flux distribution corresponds to the average for two consecutive sets of measurements. The replicate average flux distributions at a detrainment rate of 0.31 L m^{-2} s^{-1} (dark and light blue symbols and lines) were measured at the beginning and end, respectively, of the characterization period.

3.4.3. Bubble Plume Depth

Bubble plumes were generated by pumping feed air over a range of flow rates through the deeper bank of fine-porosity frits (at approximately 100 cm depth), while flows through the shallower bank of frits were set to the minimum required to prevent backflow into those frits. Subsequently, air was pumped through the shallower bank of fine-porosity frits (at approximately 60 cm depth), while flows through the deeper frits were maintained at a minimal flow. Although based on limited data, regression slopes for number production flux versus air detrainment suggest significantly higher production efficiencies for the deeper relative to the shallower bank of frits (Figure 5). The cause(s) for this apparent divergence as a function of depth cannot be determined unambiguously based on available information but two processes may have contributed.

1. Although not measured, we presume that for a given air detrainment rate, each bank of frits produced bubble plumes with similar size distributions and thus similar rise velocities. As such, at the time of bursting, surfaces of bubbles produced by the deeper bank of frits were older than those produced by the shallower bank, which would have allowed longer periods of evolution in response to surfactants. We note that sensitivity of bubble sizes to air flow rate reflects changes in the pressure at the inlet, which, at greater depth, would be higher (e.g., Burns & Zhang, 2001). However, the available evidence suggests that the influence of surfactants would have significantly muted this effect.
2. Surfaces of bubbles produced by the deeper bank of frits scavenged surfactants from a larger volume of seawater relative to those produced by the shallower bank. Thus, for a given air detrainment rate, surface-active organics in the scavenged water column may have been more rapidly depleted by plumes produced with the shallower bank relative to those produced with the deeper bank.

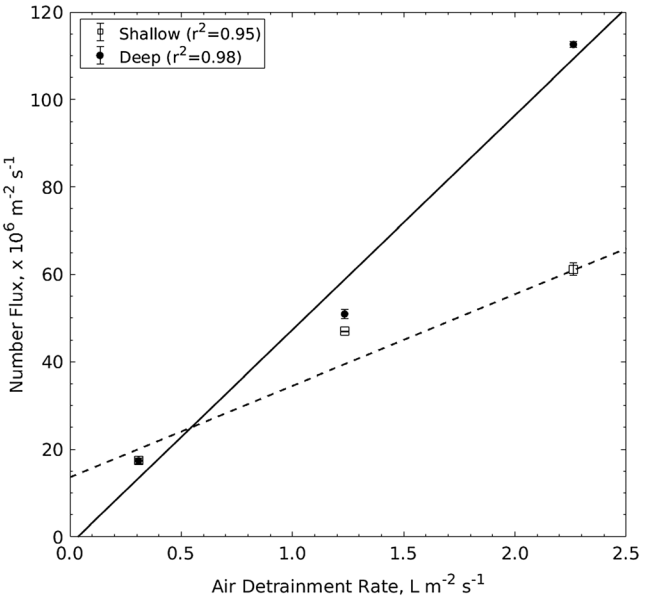

Figure 5. Total number production flux at WACS-S1 during daytime on 20 August 2012 as a function of air detrainment rate though two, independently regulated banks of fine frits positioned at average depths of approximately 60 cm (designated "shallow" and depicted with open squares and dashed line) and approximately 100 cm (designated "deep" and depicted with solid circles and line), respectively. Lines are standard linear regressions with slopes of 22.3 × 10^6 L^{-1} and 48.9 × 10^6 L^{-1}, respectively; corresponding r^2 values are in the legend. Each flux represents the average of two size-resolved flux distributions measured consecutively. Error bars depict range.

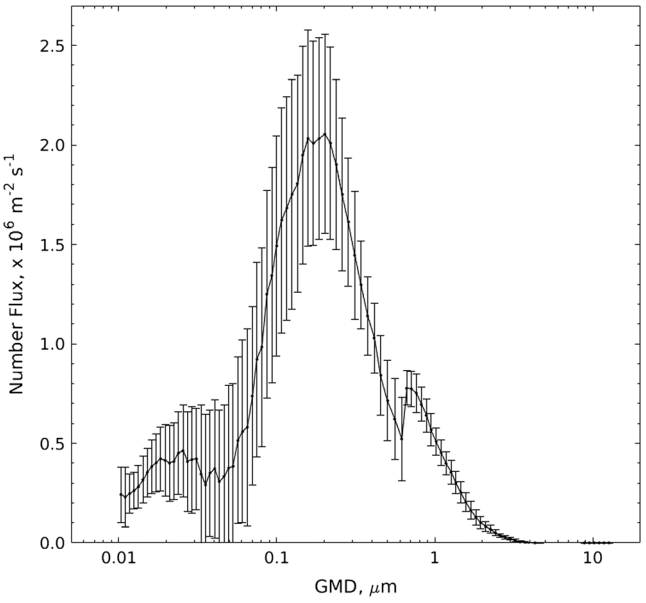

Figure 6. Mean size-resolved PMA number flux produced by the impaction of a single jet on the seawater surface at a flow rate of 2.0 L min^{-1} between 2210 on 1 June and 0840 on 2 June 2010 during CalNex. Ns for SEMS and APS are 121 and 107, respectively. Error bars depict ±1 standard deviation.

Both of these processes may have contributed to divergence in the surface-active properties of bubbles, energetics of bursting, and associated mPMA production efficiencies for plumes that evolved through deeper versus shallower depths of seawater.

3.4.4. Method of Bubble Generation: Frits Versus Jets

To quantify the incremental flux of mPMA produced via the jet(s), the measured production flux must be corrected for the background contribution from frits at the minimal air flow required to prevent flooding. This correction is based on the assumption that the background production does not vary as a function of air detrainment. As discussed previously, number production fluxes varied as linear (for fine frits) or roughly linear (for the coarse frit) functions of air detrainment rates (Figure 3), which suggests that this assumption is reasonable over the ranges of operating conditions considered here. Subtracting the background yielded the average size-resolved number flux produced by a jet depicted in Figure 6. An analogous correction could not be applied to the mass production fluxes produced by the jet because relationships between mass production fluxes and detrainment rates were highly nonlinear (Figure 3). The additional air detrainment associated with jets attenuated the background mass production flux associated with frits. Correcting the measured fluxes for the background contribution from frits in the absence of jets yielded negative residual mass fluxes produced by the jets over the upper end of the aerosol size distribution. Consequently, only the background-corrected number production fluxes can be interpreted with reasonable confidence.

Since air detrainment rates associated with jets could not be measured, the corresponding PE_{num} values could be not determined. In addition, relative to frits, less time was devoted to characterizing properties of mPMA produced with jets so insufficient information is available to evaluate diel variability. Finally, the areal cross sections of the interface through which bubble plumes detrained were variable and not quantified. Consequently, number fluxes were normalized to the cross section of the generator, which corresponds to lower limits for fluxes per unit surface area of detraining bubble plume. However, many characteristics of mPMA produced by jets do not vary as a function of the detrainment surface area and, thus, can be interpreted with confidence. For example, the shapes of background-corrected size-resolved mPMA distributions produced by jets (Figure 6) were similar to those produced by frits, although the distributions were shifted somewhat toward larger GMDs. The GMD corresponding to the peak number flux in Figure 6 is 0.171 μm, whereas those based on frits range from 0.065 to 0.108 μm (Table 3).

The mean (±standard deviation) for the total number of particles (integrated over all size bins) produced by the jet during CalNex (Figure 6, 56.8 ± 10.4 × 10^6 m^{-2} s^{-1}) fell within the range of those produced by frits under the experimental conditions evaluated during these deployments (Figure 3). However, bubble plumes generated by jets extended only about 5 cm below the air-water interface, and consequently, the average lifetimes of bubbles produced by jets were much shorter and the corresponding volume of seawater scavenged much less than for bubble plumes produced by frits (Table 1) or by many open-ocean wind waves (Deane & Stokes, 2002; Thorpe, 1982; Thorpe & Hall, 1983; Thorpe et al., 1982). Given the temporal evolution of surfactants on bubble

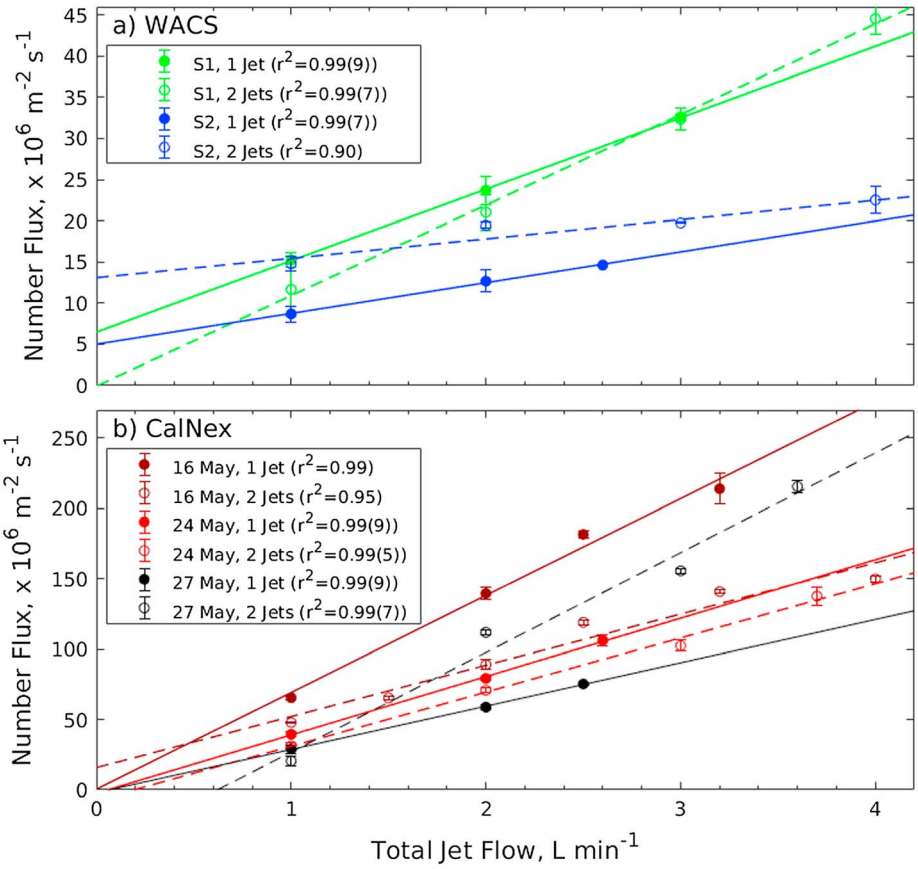

Figure 7. Total production flux of mPMA number as a function of the combined seawater flow rate through one (solid symbols and lines) or two jets (open symbols and dashed lines) (a) at WACS-S1 on 20 August 2012 (green) and at WACS-S2 on 24 August 2012 (blue) and (b) on three different days during CalNex. Lines correspond to standard linear regressions; correlation coefficients are presented in the panel legends. Each total flux represents the average of two (during WACS) or three or more (during CalNex) size-resolved flux distributions measured consecutively. Error bars depict range for WACS and ±1 standard deviation for CalNex. All characterizations were during daytime. The in-line dryer was not used during the CalNex measurements. Note that scales on *Y* axes differ.

surfaces as indicated by temporal variability in surface tension discussed in section 3.1.2, we hypothesize that for a given seawater type, mPMA OM emitted to air via the bursting of short-lived bubbles associated with shallow plumes produced by jets may be chemically distinct from that emitted via the bursting of longer-lived bubbles associated with deeper plumes produced by frits in our generator or by many wind waves at the sea surface.

Number production fluxes were linearly correlated with the seawater flow rate through both a single jet and two jets (Figure 7). Similarly, the slopes for linear regressions of number production versus jet flow were greater during the daytime at WACS-S1 relative to WACS-S2 indicating more efficient number production per unit jet flow from biologically productive water during daytime relative to oligotrophic water. Slopes also varied substantially over the range of seawater types characterized during CalNex. However, several regressions yielded intercepts that differed significantly from 0.0 suggesting nonlinearities at jet flows below 1.0 L min^{-1} (the lowest jet flow rate characterized) under some conditions. Causes for such nonlinearities are not known.

During CalNex, all characterizations of mPMA production as functions of jet number and flow rate were conducted without a dryer in-line, whereas during WACS, mPMA was dehydrated upstream of the sizing instruments. As discussed in more detail below, dehydrating mPMA either in the generator's headspace or via an in-line dryer resulted in negative bias in number concentrations. This difference in configuration of the system contributed to the relatively higher production fluxes for a given seawater flow rate through jets during CalNex relative to WACS (Figure 7).

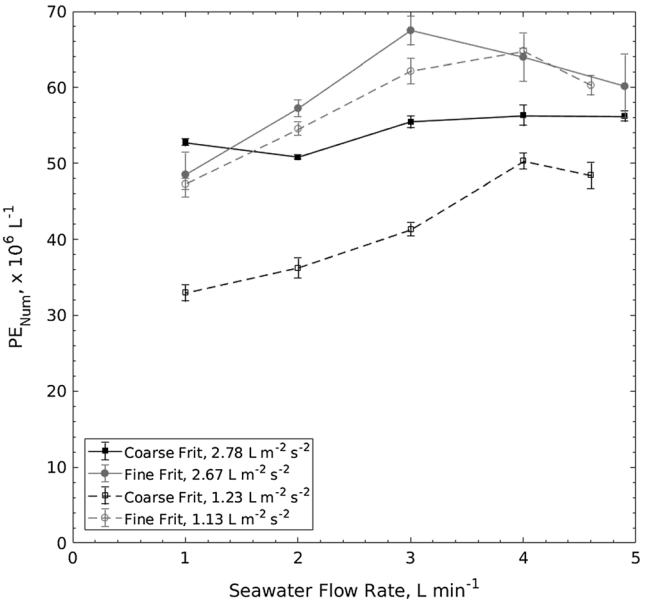

Figure 8. PE_{num} values summed over all size fractions of mPMA produced during CalNex using coarse (black square symbols and lines) and fine frits (gray round symbols and lines) at two different air detrainment rates each (specified in the legend) as a function of seawater flow rate through the generator on 17 May 2010 between 0954 and 1955. Each value corresponds to the average of three size distributions measured consecutively. Error bars depict ±1 standard deviation. The in-line dryer was not used during these measurements.

3.5. Other Operational Factors Affecting mPMA Production

3.5.1. Seawater Feed Rate

Variability in the flow rate of seawater through the generator can influence mPMA production by (1) modulating the delivery of fresh surfactant OM with associated implications for plume dynamics and (2) modulating the lifetime and associated physical properties of bubble rafts at the interface. Because the residence time of seawater in the generator (~10 min at a typical flow rate of 4 L min^{-1}) is much longer than that of individual bubbles (~2 to 10 s), variability in the seawater feed rates considered here (0 to 5 L min^{-1}) had minimal influence on bubble rise velocities and lifetimes.

For a given frit porosity and air detrainment rate during CalNex, variability in seawater feed rates to the generator between about 2.5 and 5.0 L min^{-1} had a minor to negligible influence on the corresponding PE_{num} values, whereas at lower seawater feed rates, PE_{num} values generally decreased (Figure 8). Spatial variability in properties of feed seawater over the 10 h duration of the characterization period probably contributed to the corresponding variability in PE_{num}, which precludes unambiguous interpretation of variability in PE_{num} as a function of seawater feed rate. However, in biologically productive waters at both WACS-S1 and during CalNex, when seawater flow through the generator was turned off completely, PE_{num} values decreased systematically by 26% and 43%, respectively, over periods of a few minutes (Long, Keene, Kieber, et al., 2014). These results support that hypothesis that at seawater feed rates greater than about 2.5 L min^{-1}, the delivery of the primary surfactants that modulate plume dynamics and aerosol production from biologically productive seawater exceeded rates of scavenging and removal via bubble processing resulting in minimal variability in PE_{num} values for a given set of conditions. At lower seawater feed rates, scavenging and removal of the primary surfactant reservoir via bubble processing exceeded the delivery rate of primary surfactant, revealing the transition to a secondary or background surfactant reservoir that is associated with lower mPMA production efficiencies.

3.5.2. RH Within Headspace and Sample Transmission Line

Keene et al. (2007) reported that number concentrations of mPMA measured in the headspace of the generator decreased by approximately 35% as RH in the headspace decreased from ~90% to ~50%. The authors speculated that this trend reflected increasing losses of smaller particles to surfaces as RH decreased due to electrostatic effects. Freshly produced mPMA is charged (e.g., Blanchard, 1963), and at lower RH, the static electrical relaxation time is relatively long compared to conditions at higher RH. The longer relaxation time coupled with smaller aerosol size at lower RH may have contributed to relatively greater losses to surfaces within the generator. During CalNex, a similar analysis of variability in mPMA concentrations as a function of RH in the generator's headspace with no dryer in-line upstream of the sizing instruments revealed a similar trend of comparable magnitude (not shown).

To elucidate the nature of this loss mechanism in more detail, RH within the headspace was adjusted to 80 ± 1% and size-resolved number production fluxes were measured alternately with and without the dryer in-line. The standard configuration of the SEMS used dry room air as sheath air. This configuration yielded RHs measured within the SEMS of approximately 25%, which effectively dehydrated particles immediately prior to characterization regardless of RH in the generator's headspace. Because number size distributions measured by the SEMS both with and without the dryer in-line corresponded to dry particles, differences in size distributions reflect influences of drying upstream of as opposed to drying within the instrument. In contrast, the APS used humid sample air as the sheath, and thus, differences in size distributions measured with and without the dryer in-line were driven primarily by changes in mPMA water content. Consequently, interpretation of results for this set of conditions is limited to those for the SEMS. Size-resolved number production fluxes (dry GMDs between 0.01 and 0.62 μm) using coarse or fine frits were measured at

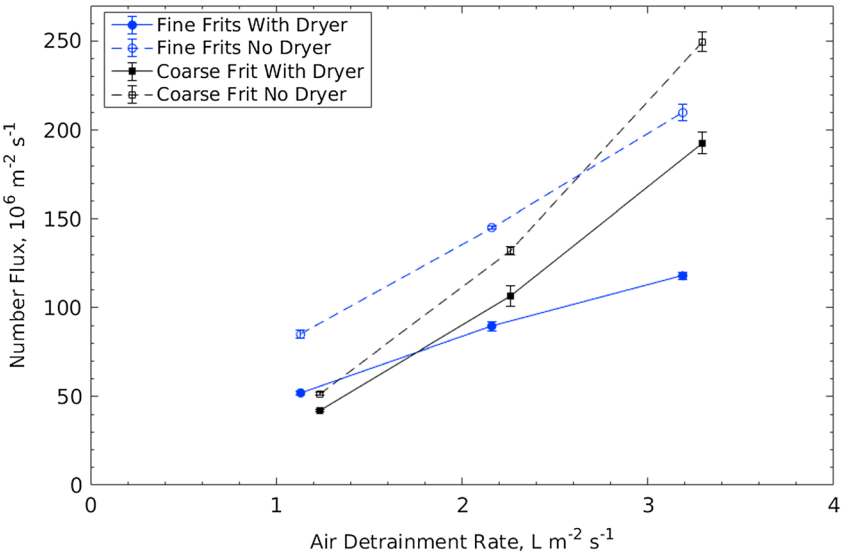

Figure 9. Total number production flux summed over the SEMS size bins (dry GMDs between 0.01 to 0.62 μm) versus air detrainment rate using fine or course frits measured with and without the dryer in-line on 1 June 2010 between 1006 and 1521 during CalNex. RH within the generator headspace was 80.3 ± 1.4%. Dry room air was used as the sheath air for the SEMS yielding RHs within the instrument of ~25%. Each flux corresponds to the average of three consecutive size distributions. Error bars depict ±1 standard deviation.

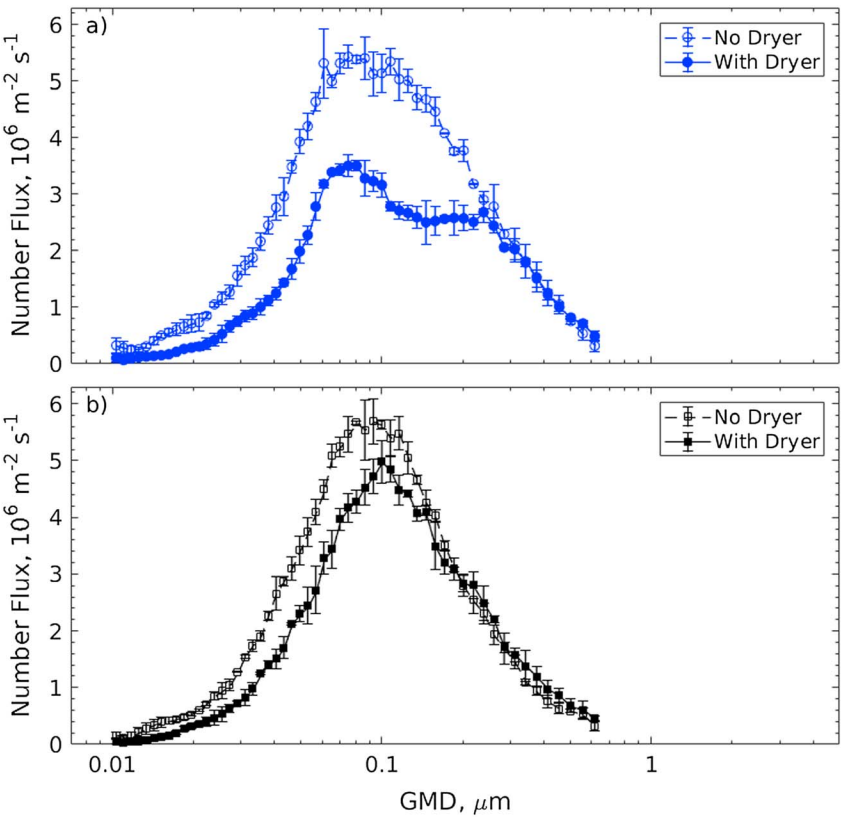

Figure 10. Examples of the average (*Ns* = 3) size-resolved number production fluxes from which the summed fluxes depicted in Figure 9 were calculated; (a) fine frits at an air detrainment rate of 2.16 L m^{-2} s^{-1} and (b) the coarse frit at an air detrainment rate of 2.26 L m^{-2} s^{-1}. Error bars depict ±1 standard deviation.

three different air detrainment rates each with either the dryer in-line or the dryer off-line (Figure 9). Total number fluxes produced using fine frits and measured downstream of the dryer ranged from 38% to 44% lower than those measured without the dryer in-line. Total number fluxes produced using the coarse frit measured downstream of the dryer ranged from 19% to 23% lower than those measured without the dryer in-line. Examples of the corresponding size-resolved fluxes (Figure 10) indicate that losses were limited to particles less than about 0.2 μm dry diameter. The relatively larger particle size distributions produced with the coarse frit than those produced with fine frits (Figure 2 and Table 3) contributed to the proportionately lower losses of particles produced with the coarse frit. It is evident that the numbers of hydrated particles that entered the dryer were significantly greater than the numbers of dry particles downstream of the dryer.

We also characterized mPMA number and mass production fluxes over a period of approximately 5.5 h with the RH of the headspace maintained at 20 ± 2%, which is well below the efflorescence RH for marine aerosol (e.g., Tang, 1997; Tang et al., 1997). The dryer was alternately placed in-line and then taken off-line for periods of approximately 20 to 30 min each. Although measured number and mass production fluxes decreased over the entire period of observation, fluxes during individual periods with the dryer in-line versus those with the dryer off-line followed the same overall trend (Figure S2). These results reveal no discernable losses of dry mPMA within the dryer, which indicates that the losses evident in Figures 9 and 10 were driven by dehydration of particles within the dryer. Taken together, the above results support the hypothesis that electrostatic effects associated with drying at low RH led to enhanced losses of particles less than about 0.2 μm dry diameter to surfaces within in the headspace, transmission line, and in-line dryer. Consequently, number production fluxes and PE_{num} values reported herein are considered lower limits. Mass production fluxes are dominated by the upper end of size distributions (Figure 2), which are not subject to significant negative artifacts of this nature (Figure 9).

3.6. Chemical Characteristics of mPMA

Because long sampling times (greater than 12 h) were required to generate sufficient mass for reliable characterization of size-segregated chemical composition, potential influences of time of day on mPMA could not be resolved. However, systematic variability in size-resolved chemical characteristics of mPMA as functions of both frit porosity and seawater type was evident (Figures 11a and 11b and Table 4). For example, during both WACS and CalNex, size-resolved mPMA was sampled over several consecutive 2 day periods at similar air detrainment rates but using fine frits on the first day and the coarse frit on the second. Results for the four sets of paired samples (at WACS-S1, at WACS-S2, and during CalNex on 28 to 30 May and on 30 May to 1 June) indicate that total Na^+ production per unit air detrained (PE_{Na+}) when using the coarse frit was higher than the corresponding value when using fine frits (Table 4). These results are consistent with the greater production of supermicron mPMA mass under otherwise similar conditions when using the coarse frit relative to fine frits (Figure 2). In contrast, production efficiencies for total OC_{we} (PE_{OCwe}) in the paired samples when using fine frits were modestly but consistently greater than those when using the coarse frit (Table 4). These relationships may reflect the smaller bubble sizes, correspondingly larger bubble surface-to-volume ratios, and thus larger surfactant-coated surface area delivered to air-water interface per unit air detrained when using fine versus coarse frits. Alternatively, corresponding differences in surface age (e.g., Table 1) may have contributed to chemical divergence in surfactant coatings and associated energetics of bubble bursting. Regardless, it is evident that the production of inorganic sea salt and OC mass varied systematically as a function of bubble size and that for each set of paired samples generated under otherwise similar conditions, relative variability on inorganic sea salt and OC_{we} resulted in greater $EF(OC_{we})$ values based on concentrations summed over all size fractions when using fine frits (Table 4).

Distributions of size-resolved $EF(OC_{we})$ for mPMA produced with frits (Figure 11c) were generally similar in shape but lower in absolute magnitude relative to those previously reported for mPMA produced from near-shore Sargasso seawater at Bermuda using fine frits positioned at similar depth (Keene et al., 2007). Based on concentrations summed over all impactor size fractions, PE_{OCwe} values for fine frits during WACS and CalNex (Table 4) overlapped the range of values (0.86 to 1.64 nmol C L^{-1}) corresponding to results reported by Keene et al. (2007). Differences in $EF(OC_{we})$ between the earlier land-based deployment versus the latter two shipboard campaigns were driven primarily by more efficient (factor of 6 based on median values) production per unit air detrained of inorganic sea-salt species, which are associated primarily with supermicron diameter size fractions (Figure 11a). Three operational factors probably

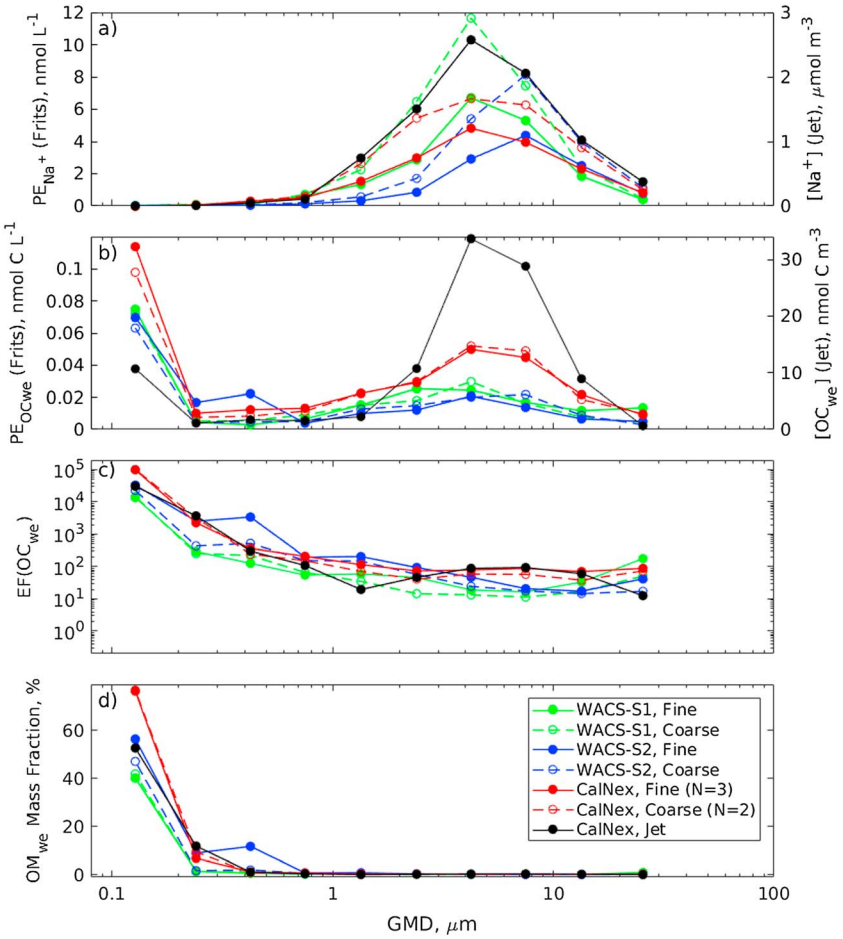

Figure 11. Size-resolved chemical characteristics of mPMA generated using fine (solid symbols and lines) and coarse frits (open symbols and dashed lines) at WACS-S1 (green), at WACS-S2 (blue), and during CalNex (red) and generated with a water jet during CalNex (black). Size distributions depicted for coarse and fine frits during CalNex correspond to averages for two and three impactor samples, respectively; other size distributions correspond to individual impactor samples. (a) Size-resolved PE_{Na+} for frits on *Y* axis and Na^+ concentration in headspace for the jet on second *Y* axis, (b) PE_{OCwe} for frits on *Y* axis and OC concentration in headspace for the jet on the second *Y* axis, (c) $EF(OC_{we})$, and (d) organic nonwater mass fraction. Times, operating conditions, and summary statistics for individual samples are reported in Table 4, and measurement uncertainties are reported in Table S1. Values less than detection limits are plotted as one half detection limits.

contributed to the relatively greater PEs for inorganic sea salt and lower $EF(OC_{we})$ values during the latter two shipboard campaigns.

1. Prior to CalNex, the original design of the generator used by Keene et al. (2007) on Bermuda was modified for shipboard deployment (Long, Keene, Kieber, et al., 2014). Overflow ports for seawater at the air-water interface were replaced with an annular space that allowed seawater exhaust to flow continuously across the entire circumference of the top edge of the seawater reservoir, which minimized bubble rafting at the interface. Based on section 3.4.2, we hypothesize that this reduction in rafting contributed to more efficient production of inorganic sea-salt mass associated with larger particles during WACS and CalNex relative to the original deployment at Bermuda.
2. Detrainment rates of bubble air used for chemical characterization runs during WACS (2.16 to 2.26 L m^{-2} s^{-1}) and CalNex (0.87 to 2.16 L m^{-2} s^{-1}) were lower than that during the original deployment (2.57 L m^{-2} s^{-1}), which also likely contributed to relatively greater PEs for sea-salt mass during the shipboard campaigns (e.g., Figure 3).
3. Finally, coarse frits, which for a given set of conditions produce relatively greater amounts of inorganic sea salt per unit air detrained, were used during about half of the chemical characterization runs during WACS and CalNex (Table 4), whereas only fine frits were used during the original deployment.

Table 4
Sample Times, Operating Conditions, and Summary of Chemical Characteristics for Size-Resolved mPMA During WACS and CalNex

Location	Frit porosity or jet	Start date, time	Stop date, time	Air detrainment rate (L m^{-2} s^{-1})	PE_{Na+}[a] (nmol L^{-1})	PE_{OCwe}[a] (nmol C L^{-1})	$EF(OC_{we})$[b]
WACS-S1	Fine	21 Aug 2012, 2047	22 Aug 2012, 1230	2.16	45.1 ± 0.6	0.456 ± 0.011	53.1
WACS-S1	Coarse	22 Aug 2012, 1523	23 Aug 2012, 0811	2.26	73.8 ± 1.1	0.426 ± 0.007	30.3
WACS-S2	Fine	24 Aug 2012, 2116	25 Aug 2012, 2119	2.16	27.9 ± 0.4	0.421 ± 0.006	100.1
WACS-S2	Coarse	25 Aug 2012, 2306	26 Aug 2012, 1832	2.26	49.6 ± 0.8	0.368 ± 0.004	49.3
CalNex	Fine	28 May 2010, 1647	29 May 2010, 0840	1.65	37.7 ± 0.7	0.778 ± 0.014	139.6
CalNex	Coarse	29 May 2010, 1130	30 May 2010, 0840	1.75	51.4 ± 0.9	0.580 ± 0.014	79.5
CalNex	Fine	30 May 2010, 1248	31 May 2010, 0850	0.87	64.1 ± 1.2	1.10 ± 0.020	117.1
CalNex	Coarse	31 May 2010, 1226	1 Jun 2010, 0839	0.98	75.1 ± 1.3	0.896 ± 0.018	76.1
CalNex	Jet[c]	1 Jun 2010 2210	2 Jun 2010, 0840	NA[d]	8438 ± 154[d]	100 ± 2.4[d]	80.4
CalNex	Fine	6 Jun 2010, 2158	7 Jun 2010, 1104	2.16	26.0 ± 0.5	0.496 ± 0.033	133.6

Note. NA, not applicable.
[a]Summed over all size fractions. [b]Based on concentrations summed over all size fractions. [c]Seawater flow at 2.0 L min^{-1} through a single jet. [d]Air detrainment rate for the jet and thus PE are not known. Concentrations in units of nmol m^{-3} are reported in place of corresponding PEs.

Although total seawater DOC concentrations were similar during these campaigns (approximately 75 μmol C L^{-1}), surfactant OM originating from local sources at Bermuda (benthic biota and surface runoff) may have also contributed to differences in bubble surface tension, bubble size and lifetime, rafting, energetics of bubble bursting, and the associated size-resolved composition of mPMA produced from near-shore relative to open-ocean seawater.

Results for paired samples of mPMA generated under similar conditions from biologically productive versus oligotrophic seawater at the two WACS stations illustrate the nature of variability in PEs for Na^+ and OC_{we} as a function of seawater type. When using fine frits, both PE_{Na+} and PE_{OCwe} at WACS-S1 were greater than those at WACS-S2 (Table 4). Similarly, when using the coarse frit, PEs for both species were also greater at WACS-S1. In addition, like those for PE_{mass}, the size distributions for PE_{Na+} at WACS-S2 were shifted toward larger particles relative to those for WACS-S1 (Figure 11a). We conclude that these differences were driven primarily by the relatively greater number and mass PEs during daytime and the corresponding shift in PE_{mass} toward relatively smaller particles during daytime at the biologically productive WACS-S1 (Figure 2) (Long, Keene, Kieber, et al., 2014).

Relative to other periods, the lower air detrainment rates at which mPMA was generated between 28 May and 1 June 2010 during CalNex were associated with higher PEs for both Na^+ and OC (Table 4). These results are generally consistent with expectations based on relationships between PE_{mass} and air detrainment rate discussed in section 3.4.2 and depicted in Figure 4. However, variability in the characteristics of seawater from which mPMA was produced during CalNex also contributed to overall variability in mPMA production (Long, Keene, Kieber, et al., 2014), and consequently, the corresponding variability in PEs for Na^+ and OC_{we} during CalNex cannot be interpreted unambiguously with respect to air detrainment rate alone.

The smallest size fraction of mPMA produced from the same seawater type using coarse and fine frits exhibited similar organic mass fractions and $EF(OC_{we})$s (Figures 11c and 11d). Although these properties of the smallest mPMA size fractions varied somewhat as a function of seawater type at WACS-S1, at WACS-S2, and during CalNex, they overlapped the ranges of previously reported values for mPMA OC_{we} (Keene et al., 2007) and total OC (Aller et al., 2017; Facchini et al., 2008; Quinn et al., 2014) produced at other locations and times. Organic mass fractions and $EF(OC_{we})$s decreased rapidly with increasing particle size. As discussed above, it is evident that the higher organic mass fractions for larger mPMA size bins reported by Keene et al. (2007) relative to those depicted in Figure 11d were driven primarily by the relatively lower production of inorganic ionic constituents during the earlier study. Decreasing cloud condensation nuclei (CCN) activity of size-resolved mPMA during WACS relative to calibration aerosol suggests that organic mass fractions increased with decreasing size over the lower ends of size distributions (100 to 40 nm dry diameter) that could not be resolved by direct measurement (Quinn et al., 2014). It is evident that $EF(OC_{we})$ based on compositions summed over all size fractions (Table 4) as well as $EF(OC_{we})$ and the corresponding organic mass

fraction for the smallest size bin (Figures 11c and 11d) did not vary systematically as a function of the phytoplankton biomass present in the parent seawater as inferred from Chl *a* concentrations (Table 1), consistent with results reported previously by Quinn et al. (2014).

The size distribution for Na^+ concentrations associated with mPMA produced with the jet was similar in shape to the size distributions of PE_{Na+} and, thus corresponding Na^+ concentrations, produced with frits (Figure 11a). However, size-resolved OC_{we} concentrations for the jet peaked in the supermicron portion of the size distribution with a lesser secondary peak associated with the smallest size fraction, whereas all size distributions of PE_{OCwe} and corresponding concentrations for frits peaked in the smallest size fraction (Figure 11b). The primary cause for this fundamental difference in the size-resolved composition of mPMA produced with the jet versus those with frits cannot be resolved unequivocally based on available information but may relate to the relatively shallow penetration depth (several centimeters) and associated differences in surface ages of bubble plumes produced by the jet relative to those produced by frits. Despite these differences, size-resolved EF(OC_{we}) and organic mass fractions for the jet fell with the range of those for frits (Figures 11c and 11d).

mPMA produced during a previous land-based deployment of the generator on Bermuda was significantly enriched by ~20% in Ca^{2+} relative to local seawater (Keene et al., 2007). In contrast, mPMA produced on ships during both WACS and CalNex was not significantly enriched in Ca^{2+}. These differences raise the possibility that non-sea-salt Ca^{2+} from local sources on Bermuda, such as $CaCO_3$ of which much of the island is composed, may have contributed to mPMA Ca^{2+} measured during the previous deployment. However, recent characterizations of mPMA produced via jet impaction from both artificial seawater and coastal seawater sampled in a Norwegian fjord also revealed significant Ca^{2+} enrichments (Salter et al., 2016). Causes for the systematic differences in results among these campaigns are not known and warrant further investigation.

4. Implications

4.1. Representativeness of Results

The WACS and CalNex results indicate that measured properties of mPMA produced under controlled conditions within the generator varied significantly as interrelated functions of (1) seawater type and, in biologically productive waters, time of day; (2) bubble injection rate, depth, size, lifetime, and surface age; (3) surfactant depletion via bubble scavenging; (4) physical properties of the air-water interface; and (5) hydration state. With the exception of the latter factor, which almost certainly reflects losses of dehydrated mPMA to surfaces within the generator or sample transition lines, the other factors vary temporally and spatially over the surface oceans as functions of solar radiation, biological productivity, the types and concentrations of surfactants, influences of surfactants on wave breaking, air entrainment as a function of sea state, and possibly influences of the surface microlayer. The inherent complexity of the system constrains the reliability of direct comparisons between results reported herein and those generated by other groups at different times and locations. In addition, comparable results for mPMA generated from natural flowing seawater are quite limited. However, during both WACS and CalNex, the NOAA Pacific Marine Environmental Laboratory generated mPMA from bubble plumes produced by pumping clean air through two stainless steel diffusion stones (2 μm porosity) suspended at a depth of 75 cm from an aerosol generator floating on the sea surface (Sea Sweep) and, subsequently, characterized physical and chemical properties of the emitted particles. When operated in parallel, the two generators yielded mPMA with similar normalized number size distributions and size-resolved organic enrichment factors (Bates et al., 2012; Quinn et al., 2014). The good agreement between these paired results based on different approaches suggests that these characteristics of mPMA are reasonably representative of those produced by ambient wind waves at comparable air detrainment rates. In addition, because the shipboard generator drew seawater from a depth of approximately 5 m, whereas Sea Sweep injected air directly into the near-surface ocean, this good agreement suggests that potential interactions involving organic surfactants associated with the sea-surface microlayer did not significantly modulate normalized size distributions or organic enrichments of mPMA produced by Sea Sweep.

Comparisons between physical properties of mPMA produced with frits versus jets reported herein relative to those of mPMA produced with frits versus breaking waves in a wave tank containing filtered coastal seawater (Prather et al., 2013) and with frits versus plunging jets during mesocosm experiments (Alpert et al., 2015) suggest that number size distributions produced with frits are typically shifted toward relatively smaller

particles. Causes for these differences are not entirely clear. As noted above, plumes produced by jets in the UVA generator were much shallower than those produced with frits or by open-ocean wind waves, which probably contributed to divergence in results. In addition, filtering coastal seawater used in the wave tank experiments reported by Prather et al. (2013) or microbial growth during the mesocosm experiments reported by Alpert et al. (2015) may have altered the natural surfactants that modulate bubble plume dynamics in and associated characteristics of mPMA produced from ambient seawater. Regardless, available evidence suggests that these differences in shapes of mPMA number size distributions may be of relatively minor importance in terms of overall environmental implications. All particles within the range of variability in centroids for frits (0.065 to 0.108 μm dry diameter, Table 3), the jet (0.171 μm dry diameter, Figure 5), and the wave tank (0.162 μm dry diameter) (Prather et al., 2013) are effective CCN (Quinn et al., 2014). In addition, following production, the composition of submicron PMA in ambient air is rapidly (seconds to minutes) modified and continues to evolve chemically over its atmospheric lifetime via condensation of gases and in situ chemical transformations (Erickson et al., 1999; Sander et al., 2003; Zhou et al., 2008). Consequently, non-sea-salt constituents contribute significantly to the nonwater mass of marine aerosol (Huebert et al., 1996; Keene et al., 2009; Savoie et al., 2002; Turekian et al., 2003). Because freshly produced PMA account for minor fractions of ambient aerosol and CCN populations over the ocean (Quinn et al., 2017), we conclude that in terms of environmental (including climatic) implications, the total number and mass production fluxes of PMA as functions of major drivers are more important than relatively minor differences in the initial shapes of size distributions.

Reliable extrapolation of results reported herein to production of ambient PMA at the ocean surface requires knowledge of the trophic state of the surface ocean and characteristics of wave breaking including the depth and volume of entrained air that detrains as small bubbles that produce particles. Because most surface waters over the global ocean are oligotrophic, results for the oligotrophic WACS-S2 are most relevant to most oceanic regions. At WACS-S2, PE_{num} values summed over mPMA size distributions generated at air detrainment rates of 2.3 and 2.2 L m^{-2} s^{-1} through coarse and fine frits, respectively, fell within a narrow range during both daytime and nighttime periods (22.4 to 26.2 × 10^6 L^{-1}, Table 3). The corresponding PE_{OCwe} values for coarse and fine frits at WACS-S2 were also similar (0.368 and 0.421 nmol C L^{-1}, respectively, Table 4). These results indicate that over the ranges of operating conditions evaluated, PE_{num} and PE_{OCwe} did not vary substantially as a function of bubble size, age, or void fraction. In addition, for air detrainment rates of less than about 2.5 L m^{-2} s^{-1}, mPMA number production fluxes for both coarse and fine frits were approximately linearly correlated with air detrainment rate (Figure 3). At higher detrainment rates, PE_{num} values for coarse frits were disproportionately greater. Taken together, the above suggests that over most of the ocean, at air detrainment rates of less than about 2.5 L m^{-2} s^{-1} within the ranges of bubble plume characteristics evaluated (size distributions and depth), the above production efficiencies for mPMA number and OC_{we} are reasonably representative of those for ambient PMA production efficiencies. Void fractions, plume depths, and detrainment rates in our generator were within ranges of values reported in the literature (Deane & Stokes, 2002; Lamarre & Melville, 1991; Thorpe & Hall, 1983). However, when air detrainment rates from the surface ocean are higher, PEs associated with ambient wind waves would likely be higher than those reported herein; when bubble plumes in the surface ocean are mixed to shallower depths, PEs would be lower; and if bubble size distributions in surface water differ substantially, PEs may also differ.

In biologically productive waters at WACS-S1, PE_{num} values at night using coarse and fine frits were similar to those for oligotrophic WACS-S2 (Table 3). Although conditions were more variable during CalNex, similar PE_{num} values were also measured at night over one diel cycle when sea state was relatively calm (Long, Keene, Kieber, et al., 2014). However, during daytime, PE_{num} values at WACS-S1 and during CalNex were generally higher than those at WACS-S2 by factors of 2 to 3 (Table 3). Again, the internal consistency of these results suggests that they are broadly representative of ambient PMA production for comparable air detrainment rates and plume dynamics.

Production efficiencies for mPMA mass as a function of air detrainment rate (Figure 3) are considerably more variable and, as described previously, highly sensitive to operating conditions and associated characteristics of the air-water interface. The generator as currently configured is analogous to a continuously breaking whitecap, whereas the available evidence presented above supports the hypothesis that PE_{mass} varies spatially and temporally over the evolution of a breaking wave. We infer that PE_{mass} values over most of the air detrainment rates characterized to date using our generator probably represent lower limits.

4.2. Comparability of mPMA Produced by Different Approaches

The process of wave breaking establishes the conditions and the total energy available for PMA production from a given seawater type. Clearly, some processes and features of the natural system are not well constrained by the method used here. Conversely, other mPMA generators cited in the text capture several important features of PMA production that are not resolvable by our system but at the cost of the representativeness of other features. Based on work by our group reported and cited herein, as well as that by other groups employing physically based marine aerosol production systems, we briefly assess the strengths and weaknesses of different approaches to provide context for improving the design and operation of mPMA generators employed in future research efforts of this nature. Although integrally interconnected, to facilitate discussion, we partition these issues somewhat arbitrarily into discrete subsections.

4.2.1. Seawater Composition

The high degree of variability in mPMA produced from different seawater types under otherwise similar conditions clearly indicates that the physics of mPMA production is sensitive to seawater composition, particularly surface-active OM (Long, Keene, Kieber, et al., 2014) (discussed in detail below). The use of frits probably limits the scope of this sensitivity to some degree since surface tension (and likely viscosity) also impacts the dynamics of plume formation, the influences of which are not captured by frits. However, the observed sensitivity to seawater composition does suggest that mPMA produced from synthetic, processed, amended, and/or coastal seawater may not be representative of production from ambient open-ocean seawater. The ability to investigate aspects of the production process over a broad range of fresh seawater types in situ is a primary strength of our system and associated variability in mPMA production represents one of the most important results of this work.

4.2.2. Air Entrainment and Bubble Plume Characteristics

The use of sintered frits to generate bubbles does not reliably capture processes involving the disintegration of entrained air into natural bubble plumes and does not produce bubble size distributions that span the full range in ambient seawater but the associated implications in terms of mPMA production are uncertain. Studies based on comparisons of mPMA produced from filtered coastal seawater in a wave tank (Prather et al., 2013) and by plunging sheets of seawater (Stokes et al., 2013) suggest that nonrepresentative bubble plumes produced by frits yield nonrepresentative size distributions of mPMA. However, the characteristics of a representative size distribution of PMA produced from natural seawater by ambient wind waves are uncertain (Quinn et al., 2015). In addition, our results indicate that under otherwise similar operating conditions in the same seawater type, coarse and fine frits yielded generally similar size-resolved and total PE_{num} values (Figure 2 and Table 3) despite large differences in bubble void fraction, size, and lifetime (Figure 1 and Table 1). These results suggest that over the ranges of conditions evaluated here, bubble size distribution alone may be less important in modulating mPMA characteristics than suggested by Prather et al. (2013) and Stokes et al. (2013). In contrast, as discussed above, plume depth does appear to be an important factor, which implies that mPMA generated via detrainment of plumes (including those produced by jets in our generator) that are much shallower than those produced by open-ocean wind waves (ranging from greater than 30 cm) (Deane & Stokes, 2002) to a meter or more (Thorpe, 1982; Thorpe & Hall, 1983; Thorpe et al., 1982) may not be entirely representative of PMA emitted over the open ocean. Physical models of mPMA production should be scaled directly to dimensions of the natural system.

4.2.3. OM Scavenging

Our results suggest that variability in the production of mPMA number, mass, and size as a function of seawater type and, in biologically productive waters, time of day over the ranges of conditions considered herein was driven primarily by variability in the associated surfactant OM in seawater. The process of OM scavenging varies as function of bubble surface area and lifetime (Blanchard & Syzdek, 1972; Skop et al., 1994) as well as the composition and concentrations of surfactants. Because organic surfactants in seawater vary spatially and temporally over wide but poorly characterized ranges of concentrations, compositions, and associated surface affinities, we assume that mPMA production from fresh, flowing seawater will yield the most representative results. In addition, our results indicate that at low or no seawater flow rates, bubble scavenging depletes surfactants in seawater reservoirs, thereby altering the physics of mPMA production. Consequently, approaches based on mPMA production from fixed-volume, nonflowing seawater reservoirs may yield nonrepresentative results.

4.2.4. Air Detrainment and Surface Processes

Our results strongly suggest that processes at the air-water interface represent a major yet poorly characterized source of variability in mPMA production. Most studies have shown that film drops are not produced by

individual bubbles smaller than about 1 mm diameter that burst on a calm surface (e.g., Lewis & Schwartz, 2004), whereas jet drops are produced by individual bursting bubbles down to about 10 μm diameter (Blanchard, 1989). However, under otherwise similar conditions, mPMA generated during our experiments via the detrainment of bubbles of different sizes in the water column (Table 1) exhibited similar size distributions of PE_{num} and PE_{mass} (Figures 2a–2d). In addition, number production fluxes for coarse frits and mass production fluxes for both frit porosities varied nonlinearly (i.e., PE_{num} and PE_{mass} varied) as a function of the detrainment flux of similarly sized bubbles (Figures 3 and 4). These results indicate that factors other than bubble size in the water column significantly influenced size-resolved mPMA production. These results are consistent with the hypothesis that bubble rafts at the air-water interface modulate size-resolved fluxes from the ocean surface. Consequently, the canonical view of film and jet drop production as a function of bubble size in the water column or on the surface may not be the most appropriate model for PMA production via bubble air that detrains through open ocean whitecaps.

Interactions at the surface are driven both by processes at the surface itself such as wind shear and bubble-bubble interactions and by the properties of the detraining bubbles at and below the surface. Previous work has characterized the process of bubble interaction at the surface as patently stochastic (Ghosh, 2004) and work investigating the lifetime and extent of bubble rafts on the surface strongly supports the hypothesis that bubble-bubble interactions at the surface modulate the particle production process significantly. It is important, then, to identify how features of more naturally representative bubble plumes and surfaces vary in response to major drivers. As designed, our system and most others do not permit direct characterization of interactions at the air-water surface over relevant ranges of conditions. However, several groups have made important strides in understanding such multibody processes among bubbles at the surface (Callaghan et al., 2013; Collins et al., 2014; Ghosh, 2004; Modini et al., 2013; Salter et al., 2011, 2014; Stefan & Szeri, 1999). We conclude that greater effort should be focused on resolving the nature of the important but poorly characterized processes at the air-water interface that modulate mPMA production.

4.2.5. Size-Resolved mPMA Concentrations and Characteristics Versus Fluxes

Several mPMA generators allow unprecedented resolution in characterizing important chemical and physical properties of size-resolved mPMA (e.g., Bates et al., 2012; Collins et al., 2014; Prather et al., 2013; Quinn et al., 2014). Although such characterizations represent useful contributions in their own right, the corresponding fluxes as functions of major drivers cannot be reliably estimated based on these approaches, which limits the applicability of results in parameterizing PMA production in models. In addition, several published approaches focus on characterizing properties of only the lower ends of the aerosol size distribution that dominate number fluxes but ignore the upper ends of the size distribution that dominate mass fluxes (e.g., Tyree et al., 2007). Both the lower and upper portions of the marine aerosol size distribution significantly impact the composition, chemical evolution, and environmental (including climatic) feedbacks of the marine troposphere (e.g., Long, Keene, Easter, et al., 2014). Consequently, we encourage the community to adopt approaches that allow characterization of the chemical and physical properties as well as fluxes of mPMA over the full size distribution of ambient marine aerosol.

Available evidence summarized above demonstrates the sensitivity of mPMA production to both ranges of environmental variables as well as aspects of the design and operation of aerosol generation systems. These results provide useful context for ongoing efforts to improve the representativeness of mPMA produced by these devices. To the extent possible, future efforts should include direct intercomparison of performance based on different approaches operated in parallel.

5. Summary

Like all models, both physical and numerical, the approach employed to generate results reported herein does not reliably capture all aspects of the subject system. However, this approach does allow many factors that modulate variability in mPMA production from ambient seawater to be evaluated explicitly over relevant ranges of conditions. Results yield important insights regarding the underlying processes that drive production of PMA from the surface ocean and, thereby, provide useful context for improving parameterization of PMA production in regional and global models. The major conclusions of this study are as follows:

1. For a given set of conditions during daytime, bubble sizes were larger, rise velocities faster, steady state void fractions lower, and surface ages at the time of bursting younger in oligotrophic relative to

biologically productive seawater. These relationships were driven primarily by distinct concentrations and/or speciation of surfactant OM and the associated properties in these different seawater types.

2. Bubble processing reduced total DOC concentrations in oligotrophic seawater by an average of 30% but had no measurable influence on DOC concentrations in biologically productive waters. We infer that the primary surfactants coating bubbles in oligotrophic seawater were converted to particulate, possibly gel-like, material of sufficient size (0.2 μm diameter) and lifetime (minutes) to be removed via filtration prior to DOC analysis, whereas those in biologically productive waters were not.
3. For a given set of conditions, PE_{num} and PE_{mass} values for biologically productive seawater during daytime were greater than those for biologically productive seawater at night or for oligotrophic seawater. In biologically productive waters, the mPMA size bin associated with the highest PE_{mass} during daytime was shifted toward smaller particles relative to nighttime. These differences support the hypothesis that sunlight-mediated biogenic surfactants in productive waters modulate mPMA production via interaction with bubble plumes.
4. mPMA number fluxes produced with fine frits were linearly correlated with air detrainment rates and, for detrainment rates less than about 2 L m^{-2} s^{-1}, were similar to those produced with the coarse frit. At higher air detrainment rates, number fluxes generated with the coarse frit were proportionately greater and the magnitude of divergence increased with increasing detrainment rate. The greater energy dissipated at the interface by larger faster-rising bubbles produced with the coarse frit may have contributed to the divergence at higher detrainment rates.
5. mPMA mass fluxes per unit air detrained (i.e., PE_{mass}) decreased with increasing air detrainment rates. We hypothesize that increased areal coverage and thickness of surface bubble rafts with increasing air detrainment rates attenuated the corresponding injection of jet droplets and associated mPMA mass across the air-water interface. These results suggest that the emission of PMA mass from the surface ocean may be driven by relatively small fractions of entrained air that detrain as individual bubbles around the perimeter or during the dissipation of fully developed whitecaps.
6. Based on slopes for PE_{num} versus air detrainment rates, PE_{num} values for frits positioned at an average depth of approximately 100 cm were greater by a factor of about 2 relative to those for frits positioned at an average depth of 60 cm. These results imply the number production efficiencies vary substantially as a function of the depth to which bubble plumes are mixed into the surface ocean.
7. The relative shapes of size-resolved mPMA distributions produced by the jet were similar to those produced by frits, although the jet distributions were shifted toward larger GMDs.
8. Relative to those for coarse frits, PE_{Na+} values for fine frits based on concentrations summed over all size fractions were about 40% lower and the corresponding PE_{OCwe} values were about 10% higher. Consequently, the corresponding EF(OC_{we}) values for fine frits were greater than those for the coarse frit.
9. For all conditions characterized, size-resolved concentrations of OC_{we} based on frits peaked in the smallest size fraction (GMD = 0.13 μm) whereas that for the jet peaked in the supermicron size range (GMD = 4.2 μm). However, the corresponding organic mass fractions and EF(OC_{we}) values for mPMA based on the coarse frit, fine frits, and the jet exhibited generally similar size-dependent variability over a wide range in Chl *a* concentrations.

Taken together, results of this study indicate the physical production of PMA number and mass from the ocean surface varies systematically as interrelated functions of seawater type and, in biologically productive waters, time of day; bubble injection rate, depth, size, and surface age; and physical characteristics of the air-water interface. In contrast, size-resolved organic enrichments and mass fractions are relatively invariant.

Acknowledgments

We thank G. Henderson, I. Tyssebotn, D. Coffman, K. Schulz, D. Hamilton, J. Johnson, and M. Haserodt for their assistance in sample collection and analysis; V. Trainer for the loan and calibration of the fluorometer; and the captains and crews of the UNOLS R/V *Atlantis* and the NOAA R/V *Ronald H. Brown* for logistical support in the field. Three anonymous reviewers provided helpful suggestions for improving the original manuscript. Primary financial support for this work was provided by the U.S. National Science Foundation through awards to the University of Virginia (OCE-0948420 and OCE-1129836), State University of New York, College of Environmental Science and Forestry (OCE-0948216 and OCE-1129896), Scripps Institution of Oceanography (OCE-1129580), and Harvard University (AGS-1252755). Additional support was provided by the NOAA Atmospheric Composition and Climate Program. J. S. Reid's contribution to this effort was supported by the Naval Research Laboratory Base Program. Data recorded by the ships' crews during CalNex and WACS (position; temperature, salinity, and Chl *a* concentration in seawater; and solar radiation) are posted at https://saga.pmel.noaa.gov/data/. Other data sets are posted in the UCSD Library Digital Collections (Frossard et al., 2017a, 2017b).

References

Adamson, A. W., & Gast, A. P. (1990). *Physical chemistry of surfaces*. New York: Wiley.

Aller, J. Y., Radway, J. C., Kilthau, W. P., Bothe, D. W., Wilson, T. W., Vaillancourt, R. D., … Knopf, D. A. (2017). Size-resolved characterization of the polysaccharidic and proteinaceous components of sea spray aerosol. *Atmospheric Environment*, *154*, 331–347. https://doi.org/10.1016/j.atmosenv.2017.01.053

Alpert, P. A., Kilthau, W. P., Bothe, D. W., Radway, J. C., Aller, J. Y., & Knopf, D. A. (2015). The influence of marine microbial activities on aerosol production: A laboratory mesocosm study. *Journal of Geophysical Research: Atmospheres*, *120*, 8841–8860. https://doi.org/10.1002/2015JD023469

Andreas, E. L. (1998). A new sea spray generation function for wind speeds up to 32 m s^{-1}. *Journal of Physical Oceanography*, *28*(11), 2175–2184. https://doi.org/10.1175/1520-0485(1998)028%3C2175:ANSSGF%3E2.0.CO;2

Barber, R. T. (1966). Interaction of bubbles and bacteria in the formation of organic aggregates in sea-water. *Nature*, *211*(5046), 257–258. https:doi.org/10.1038/211257a0

Bates, T. S., Quinn, P. K., Frossard, A. A., Russell, L. M., Hakala, J., Petäjä, T., … Keene, W. C. (2012). Measurements of ocean derived aerosol off the coast of California. *Journal of Geophysical Research*, *117*, D00V15. https://doi.org/10.1029/2012JD017588

Beard, K. V., & Ochs, H. T. (1993). Warm-rain initiation: An overview of microphysical mechanisms. *Journal of Applied Meteorology*, *32*(4), 608–625. https://doi.org/10.1175/1520-0450(1993)032%3C0608:WRIAOO%3E2.0.CO;2

Birch, M. E., & Cary, R. A. (1996). Elemental carbon-based method for monitoring occupational exposures to particulate diesel exhaust. *Aerosol Science and Technology*, *25*(3), 221–241. https://doi.org/10.1080/02786829608965393

Blanchard, D. C. (1963). The electrification of the atmosphere by particles from bubbles in the sea. *Progress in Oceanography*, *1*, 73–202. https://doi.org/10.1016/0079-6611(63)90004-1

Blanchard, D. C. (1989). The size and height to which jet droplets are injected from bursting bubbles in seawater. *Journal of Geophysical Research*, *94*(C8), 10,999–11,002. https://doi.org/10.1029/JC094iC08p10999

Blanchard, D. C., & Syzdek, L. D. (1972). Concentration of bacteria in jet drops from bursting bubbles. *Journal of Geophysical Research*, *77*(27), 5087–5099. https://doi.org/10.1029/JC077i027p05087

Blanchard, D. C., & Woodcock, A. H. (1980). The production, concentration and vertical distribution of the sea-salt aerosol. *Annals of the New York Academy of Sciences*, *338*(1 Aerosols), 330–347. https://doi.org/10.1111/j.1749-6632.1980.tb17130.x

Boyce, S. G. (1954). The salt spray community. *Ecological Monograms*, *24*(1), 29–67. https://doi.org/10.2307/1943510

Burns, S. E., & Zhang, M. (2001). Effects of system parameters on the physical characteristics of bubbles produced through air sparging. *Environmental Science & Technology*, *35*(1), 204–208. https://doi.org/10.1021/es001157u

Callaghan, A., de Leeuw, G., Cohen, L., & O'Dowd, C. D. (2008). Relationship of oceanic whitecap coverage to wind speed and wind history. *Geophysical Research Letters*, *35*, L23609. https://doi.org/10.1029/2008GL036165

Callaghan, A. H., Deane, G. B., & Stokes, M. D. (2013). Two regimes of laboratory whitecap foam decay: Bubble-plume controlled and surfactant stabilized. *Journal of Physical Oceanography*, *43*(6), 1114–1126. https://doi.org/10.1175/JPO-D-12-0148.1

Clarke, A. D., Freitag, S., Simpson, R. M. C., Hudson, J. G., Howell, S. G., Brekhovskikh, V. L., … Zhou, J. (2013). Free troposphere as a major source of CCN for the equatorial pacific boundary layer: Long-range transport and teleconnections. *Atmospheric Chemistry and Physics*, *13*(15), 7511–7529. https://doi.org/10.5194/acp-13-7511-2013

Clarke, A. D., Owens, S. R., & Zhou, J. (2006). An ultrafine sea-salt flux from breaking waves: Implications for cloud condensation nuclei in the remote marine atmosphere. *Journal of Geophysical Research*, *111*, D06202. https://doi.org/10.1029/2005JD006565

Collins, D. B., Zhao, D. F., Ruppel, M. J., Laskina, O., Grandquist, J. R., Modini, R. L., … Prather, K. A. (2014). Direct aerosol chemical composition measurements to evaluate the physicochemical differences between controlled sea spray aerosol generation schemes. *Atmospheric Measurement Techniques*, *7*(11), 3667–3683. https://doi.org/10.5194/amt-7-3667-2014

Deane, G. B., & Stokes, M. D. (2002). Scale dependence of bubble creation mechanisms in breaking waves. *Nature*, *418*(6900), 839–844. https://doi.org/10.1038/nature00967

de Leeuw, G., Andreas, E. L., Anguelova, M. D., Fairall, C. W., Lewis, E. R., O'Dowd, C., … Schwartz, S. E. (2011). Production flux of sea spray aerosol. *Reviews of Geophysics*, *49*, RG2001. https://doi.org/10.1029/2010RG000349

Duce, R. A., Winchester, J. W., & Van Nahl, T. W. (1965). Iodine, bromine, and chlorine in the Hawaiian marine atmosphere. *Journal of Geophysical Research*, *70*(8), 1775–1799. https://doi.org/10.1029/JZ070i008p01775

Erickson, D. J., Seuzaret, C., Keene, W. C., & Gong, S. L. (1999). A general circulation model based calculation of HCl and $ClNO_2$ production from sea salt dechlorination: Reactive chlorine emissions inventory. *Journal of Geophysical Research*, *104*(D7), 8347–8372. https://doi.org/10.1029/98JD01384

Eriksson, E. (1960). The yearly circulation of chloride and sulfur in nature: Meteorological, geochemical and pedological implications. Part II. *Tellus*, *12*, 29–67.

Facchini, M. C., Rinaldi, M., Decesari, S., Carbone, C., Finessi, E., Mircea, M., … O'Dowd, C. D. (2008). Primary submicron marine aerosol dominated by insoluble organic colloids and aggregates. *Geophysical Research Letters*, *35*, L17814. https://doi.org/10.1029/2008GL034210

Feingold, G., Cotton, W. R., Kreidenweis, S. M., & Davis, J. T. (1999). The impact of giant cloud condensation nuclei on drizzle formation in stratocumulus: Implications for cloud radiative properties. *Journal of the Atmospheric Sciences*, *56*(24), 4100–4117. https://doi.org/10.1175/1520-0469(1999)056%3C4100:TIOGCC%3E2.0.CO;2

Frossard, A. A., Russell, L. M., Burrows, S. M., Elliott, S. M., Bates, T. S., & Quinn, P. K. (2014). Sources and composition of submicron organic mass in marine aerosol particles. *Journal of Geophysical Research: Atmospheres*, *119*, 12,977–13,003. https://doi.org/10.1002/2014JD021913

Frossard, A. A., Russell, L. M., Maben, J. R., Long, M. S., Keene, W. C., Reid, J. S., … Bates, T. S. (2017a). Measurements of generated and ambient marine aerosol particles in August 2012 on board the R/V *Ronald H. Brown* during the Western Atlantic Climate Study (WACS), UC San Diego Library Digital Collections. https://doi.org/10.6075/J04F1NNX

Frossard, A. A., Russell, L. M., Maben, J. R., Long, M. S., Keene, W. C., Reid, J. S., … T. S. Bates (2017b). Measurements of generated and ambient marine aerosol particles in May and June 2010 on board the R/V *Atlantis* during the California Nexus (CalNex) Experiment, UC San Diego Library Digital Collections. https://doi.org/10.6075/J00P0WX6

Gantt, B., & Meskhidze, N. (2013). The physical and chemical characteristics of marine primary organic aerosol: A review. *Atmospheric Chemistry and Physics*, *13*(8), 3979–3996. https://doi.org/10.5194/acp-13-3979-2013

Gaston, C. J., Furutani, H., Guazzotti, S. A., Coffee, K. R., Bates, T. S., Quinn, P. K., … Prather, K. A. (2011). Unique ocean-derived particles serve as a proxy for changes in ocean chemistry. *Journal of Geophysical Research*, *116*, D18310. https://doi.org/10.1029/2010JD015289

Ghosh, P. (2004). Coalescence of air bubbles at air-water interface. *Chemical Engineering Research and Design*, *82*(7), 849–854. https://doi.org/10.1205/0263876041596715

Gong, S. L. (2003). Canadian aerosol module: A size-segregated simulation of atmospheric aerosol processes for climate and air quality models 1. Module development. *Journal of Geophysical Research*, *108*(D1), 4007. https://doi.org/10.1029/2001JD002002

Hansell, D. A. (2013). Recalcitrant dissolved organic carbon fractions. *Annual Review of Marine Science*, *5*(1), 421–445. https://doi.org/10.1146/annurev-marine-120710-100757

Haywood, J. M., Ramaswamy, V., & Soden, B. J. (1999). Tropospheric aerosol climate forcing in clear-sky satellite observations over oceans. *Science*, *283*(5406), 1299–1303. https://doi.org/10.1126/science.283.5406.1299

Hoffman, E. J., & Duce, R. A. (1976). Factors influencing the organic carbon content of marine aerosols: A laboratory study. *Journal of Geophysical Research*, *81*(21), 3667–3670. https://doi.org/10.1029/JC081i021p03667

Holcomb, C. D., & Zollweg, J. A. (1992). Improved differential bubble pressure surface tensiometer. *Journal of Colloid and Interface Science*, *154*(1), 51–65. https://doi.org/10.1016/0021-9797(92)90077-Y

Huebert, B. J., Zhuang, L., Howell, S., Noone, K., & Noone, B. (1996). Sulfate, nitrate, methanesulfonate, chloride, ammonium, and sodium measurements from ship, island, and aircraft during the Atlantic stratocumulus transition experiment/marine aerosol gas exchange. *Journal of Geophysical Research*, *101*(D2), 4413–4423. https://doi.org/10.1029/95JD02044

Keene, W. C., Long, M. S., Pszenny, A. A. P., Sander, R., Maben, J. R., Wall, A. J., … Schrems, O. (2009). Latitudinal variation in the multiphase chemical processing of inorganic halogens and related species over the eastern North and South Atlantic Oceans. *Atmospheric Chemistry and Physics*, *9*(19), 7361–7385. https://doi.org/10.5194/acp-9-7361-2009

Keene, W. C., Maring, H., Maben, J. R., Kieber, J., Pszenny, A. A. P., Dahl, E. E., … Sander, R. (2007). Chemical and physical characteristics of nascent aerosols produced by bursting bubbles at a model air-sea interface. *Journal of Geophysical Research*, *112*, D21202. https://doi.org/10.1029/2007JD008464

Keene, W. C., Pszenny, A. A. P., Galloway, J. N., & Hawley, M. E. (1986). Sea-salt corrections and interpretation of constituent ratios in marine precipitation. *Journal of Geophysical Research*, *91*(D6), 6647–6658. https://doi.org/10.1029/JD091iD06p06647

Keene, W. C., Sander, R., Pszenny, A. A. P., Vogt, R., Crutzen, P. J., & Galloway, J. N. (1998). Aerosol pH in the marine boundary layer: A review and model evaluation. *Journal of Aerosol Science*, *29*(3), 339–356. https://doi.org/10.1016/S0021-8502(97)10011-8

Keene, W. C., Talbot, R. W., Andreae, M. O., Beecher, K., Berresheim, H., Castro, M., … Winiwarter, W. (1989). An intercomparison of measurement systems for vapor- and particulate-phase concentrations of formic and acetic acids. *Journal of Geophysical Research*, *94*(D5), 6457–6471. https://doi.org/10.1029/JD094iD05p06457

Kieber, D. J., Keene, W. C., Frossard, A. A., Long, M. S., Russell, L. M., Maben, J. R., … Bates, T. S. (2016). Coupled ocean-atmosphere loss of marine refractory dissolved organic carbon. *Geophysical Research Letters*, *43*, 2765–2772. https://doi.org/10.1002/2016GL068273

Lafon, C., Piazzola, J., Forget, P., & Despiau, S. (2007). Whitecaps coverage in coastal environment for steady and unsteady wave field conditions. *Journal of Marine Science*, *66*, 38–46.

Lamarre, E., & Melville, W. K. (1991). Air entrainment and dissipation in breaking waves. *Nature*, *351*(6326), 469–472. https://doi.org/10.1038/351469a0

Levin, Z., Teller, A., Ganor, E., & Yin, Y. (2005). On the interactions of mineral dust, sea-salt particles, and clouds: A measurement and modeling study from the Mediterranean Israeli Dust Experiment campaign. *Journal of Geophysical Research*, *110*, D20202. https://doi.org/10.1029/2005JD005810

Lewis, E. R., & Schwartz, S. E. (2004). *Sea salt aerosol production: Mechanisms, methods, measurements, and models—A critical review*. Washington, DC: American Geophysical Union. https://doi.org/10.1029/GM152

Long, M. S., Keene, W. C., Easter, R. C., Sander, R., Liu, X., Kerkweg, A., & Erickson, D. (2014). Sensitivity of tropospheric chemical composition to halogen-radical chemistry using a fully coupled size-resolved multiphase chemistry-global climate system: Halogen distributions, aerosol composition, and sensitivity of climate-relevant gases. *Atmospheric Chemistry and Physics*, *14*, 3397–3425. https://doi.org/10.5194/acp-14-3397-2014

Long, M. S., Keene, W. C., Kieber, D. J., Erickson, D. J., & Maring, H. (2011). A sea-state based source function for size- and composition-resolve marine aerosol production. *Atmospheric Chemistry and Physics*, *11*(3), 1203–1216. https://doi.org/10.5194/acp-11-1203-2011

Long, M. S., Keene, W. C., Kieber, D. J., Frossard, A. A., Russell, L. M., Maben, J. R., … Bates, T. S. (2014). Light-enhanced primary marine aerosol production from biologically productive seawater. *Geophysical Research Letters*, *41*, 2661–2670. https://doi.org/10.1002/2014GL059436

Marple, V. A., Rubow, K. L., & Behm, S. M. (1991). A Micro-orifice Uniform Deposit Impactor (MOUDI): Description, calibration, and use. *Aerosol Science and Technology*, *14*(4), 434–446. https://doi.org/10.1080/02786829108959504

Mårtensson, E. M., Nilsson, E. D., de Leeuw, G., Cohen, L. H., & Hansson, H. C. (2003). Laboratory simulations and parameterization of the primary marine aerosol production. *Journal of Geophysical Research*, *108*(D9), 4297. https://doi.org/10.1029/2002JD002263

Meskhidze, N., Petters, M. D., Tsigaridis, K., Bates, T., O'Dowd, C., Reid, J., … Zorn, S. R. (2013). Production mechanisms, number concentration, size distribution, chemical composition, and optical properties of sea spray aerosols. *Atmospheric Science Letters*, *14*(4), 207–213. https://doi.org/10.1002/asl2.441

Modini, R. L., Russell, L. M., Deane, G. B., & Stokes, M. D. (2013). Effect of soluble surfactant on bubble persistence and bubble-produced aerosol particles. *Journal of Geophysical Research*, *118*, 1388–1400. https://doi.org/10.1002/jgrd.50186

Monahan, E. C. (1968). Sea spray as a function of low elevation wind speed. *Journal of Geophysical Research*, *73*(4), 1127–1137. https://doi.org/10.1029/JB073i004p01127

Monahan, E. C., & O'Muircheartaigh, I. G. (1986). Whitecaps and the passive remote sensing of the ocean surface. *International Journal of Remote Sensing*, *7*(5), 627–642. https://doi.org/10.1080/01431168608954716

Murphy, D. M., Anderson, J. R., Quinn, P. K., McInnes, L. M., Brechtel, F. J., Kreidenweis, S. M., … Buseck, P. R. (1998). Influence of sea-salt on aerosol radiative properties in the Southern Ocean marine boundary layer. *Nature*, *392*(6671), 62–65. https://doi.org/10.1038/32138

Myhre, G., Stordal, F., Johnsrud, M., Diner, D. J., Geogdzhayev, I. V., Haywood, J. M., … Wang, M. (2005). Intercomparison of satellite retrieved aerosol optical depth over ocean during the period September 1997 to December 2000. *Atmospheric Chemistry and Physics*, *5*(6), 1697–1719. https://doi.org/10.5194/acp-5-1697-2005

Myhre, G., Stordal, F., Johnsrud, M., Ignatov, A., Mishchenko, M. I., Geogdzhayev, I. V., … Holben, B. (2004). Intercomparison of satellite retrieved aerosol optical depth over the ocean. *Journal of the Atmospheric Sciences*, *61*(5), 499–513. https://doi.org/10.1175/1520-0469(2004)061%3C0499:IOSRAO%3E2.0.CO;2

Norris, S. J., Brooks, I. M., & Salisbury, D. J. (2013). A wave roughness Reynolds number parameterization of the sea spray source flux. *Geophysical Research Letters*, *40*, 4415–4419. https://doi.org/10.1002/grl.50795

O'Dowd, C. D., Facchini, M. C., Cavalli, F., Ceburnis, D., Mircea, M., Decesari, S., … Putaud, J.-P. (2004). Biogenically driven organic contribution to marine aerosol. *Nature*, *431*(7009), 676–680. https://doi.org/10.1038/nature02959

O'Dowd, C. D., Langmann, B., Varghese, S., Scannell, C., Ceburnis, D., & Facchini, M. C. (2008). A combined organic-inorganic sea-spray source function. *Geophysical Research Letters*, *35*, L01801. https://doi.org/10.1029/2007GL030331

Porter, J. N., & Clarke, A. D. (1997). Aerosol size distribution models based on in situ measurements. *Journal of Geophysical Research*, *102*(D5), 6035–6045. https://doi.org/10.1029/96JD03403

Prather, K. A., Bertram, T. H., Grassian, V. H., Deane, G. B., Stokes, M. D., DeMott, P. J., … Zhao, D. (2013). Bringing the ocean into the laboratory to probe the chemical complexity of sea spray aerosol. *Proceedings of the National Academy of Sciences*, *110*(19), 7550–7555. https://doi.org/10.1073/pnas.1300262110

Quinn, P. K., Bates, T. S., Schulz, K. S., Coffman, D. C., Frossard, A. A., Russell, L. M., … Kieber, D. J. (2014). Contribution of sea surface carbon pool to organic matter enrichment in nascent sea spay aerosol. *Nature Geoscience*, *7*(3), 228–232. https://doi.org/10.1038/NGEO2092

Quinn, P. K., & Coffman, D. J. (1998). Local closure during the first Aerosol Characterization Experiment (ACE): Aerosol mass concentration and scattering and backscattering coefficients. *Journal of Geophysical Research*, *103*(D13), 16575–16596. https://doi.org/10.1029/97JD03757

Quinn, P. K., Coffman, D. J., Johnson, J. E., Upchurch, L. M., & Bates, T. S. (2017). Sea spray aerosol is a small fraction of marine boundary layer cloud condensation nuclei. *Nature Geoscience*, *10*(9), 674–679. https://doi.org/10.1038/ngeo3003

Quinn, P. K., Collins, D. B., Grassian, V. H., Prather, K. A., & Bates, T. S. (2015). Chemistry and related properties of freshly emitted sea spray aerosol. *Chemical Reviews*, *115*(10), 4383–4399. https://doi.org/10.1021/cr500713g

Reid, J. S., Brooks, B., Crahan, K. K., Hegg, D. A., Eck, T. F., O'Neill, N., … Anderson, K. D. (2006). Reconciliation of coarse mode sea-salt aerosol particle size measurements and parameterizations at a subtropical ocean receptor site. *Journal of Geophysical Research*, *111*, D02202. https://doi.org/10.1029/2005JD006200

Reid, J. S., Hyer, E. J., Johnson, R., Holben, B. N., Yokelson, R. J., Zhang, J., … Liew, S. C. (2013). Observing and understanding the Southeast Asian aerosol system by remote sensing: An initial review and analysis for the Seven Southeast Asian Studies (7SEAS) program. *Atmospheric Research*, *122*, 403–468. https://doi.org/10.1016/j.atmosres.2012.06.005

Reid, J. S., Jonsson, H., Smith, M., & Smirnov, A. (2001). Evolution of the vertical profile and flux of large sea-salt particles in a coastal zone. *Journal of Geophysical Research*, *106*, 12,038–12,053.

Reid, J. S., & Peters, T. M. (2007). Update to "reconciliation of coarse mode sea-salt aerosol particle size measurements and parameterizations at a subtropical ocean receptor site" regarding the use of aerodynamic particle sizers in marine environments. *Journal of Geophysical Research*, *112*, D04202. https://doi.org/10.1029/2006JD007501

Sadhal, S. S., Ayyaswamy, P. S., & Chung, J. N. (1997). Formation and breakup of bubbles and drops. In S. S. Sadhal, P. S. Ayyaswamy, & J. N. Chung (Eds.), *Transport phenomena with drops and bubbles, mechanical engineering series* (pp. 311–401). New York: Springer-Verlag. https://doi.org/10.1007/978-1-4612-4022-8_7

Salter, M. E., Hamacher-Barth, E., Leck, C., Werner, J., Johnson, C. M., Riipinen, I., … Zieger, P. (2016). Calcium enrichment in sea spray aerosol particles. *Geophysical Research Letters*, *43*, 8277–8285. https://doi.org/10.1002/2016GL070275

Salter, M. E., Nilsson, E. D., Butcher, A., & Bilde, M. (2014). On the seawater temperature dependence of the sea spray aerosol generated by a continuous plunging jet. *Journal of Geophysical Research: Atmospheres*, *119*, 9052–9072. https://doi.org/10.1002/2013JD021376

Salter, M. E., Upstill-Goddard, R. C., Nightingale, P. D., Archer, S. D., Blomquist, B., Ho, D. T., … Yang, M. (2011). Impact of an artificial surfactant release on air-sea gas fluxes during Deep Ocean Gas Exchange Experiment II. *Journal of Geophysical Research: Oceans*, *116*, C11016. https://doi.org/10.1029/2011JC007023

Salter, M. E., Zieger, P., Acosta Navarro, J. C., Grythe, H., Kirkevåg, A., Rosati, B., … Nilsson, E. D. (2015). An empirically derived inorganic sea spray source function incorporating sea surface temperature. *Atmospheric Chemistry and Physics*, *15*(19), 11,047–11,066. https://doi.org/10.5194/acp-15-11047-2015

Sander, R., Keene, W. C., Pszenny, A. A. P., Arimoto, R., Ayers, G. P., Baboukas, V., … van Dingenen, R. (2003). Inorganic bromine in the marine boundary layer: A critical review. *Atmospheric Chemical and Physics*, *3*(5), 1301–1336. https://doi.org/10.5194/acp-3-1301-2003

Savoie, D. L., Arimoto, R., Keene, W. C., Prospero, J. M., Duce, R. A., & Galloway, J. N. (2002). Marine biogenic and anthropogenic contributions to non-sea-salt sulfate in the marine boundary layer over the North Atlantic Ocean. *Journal of Geophysical Research*, *107*(D18), 4356. https://doi.org/10.1029/2001JD000970

Sessions, W. R., Reid, J. S., Benedetti, A., Colarco, P. R., da Silva, A., Lu, S., … Westphal, D. L. (2015). Development towards a global operational aerosol consensus: Basic climatological characteristics of the International Cooperative for Aerosol Prediction Multi-Model Ensemble (ICAP-MME). *Atmospheric Chemistry and Physics*, *15*(1), 335–362. https://doi.org/10.5194/acp-15-335-2015

Shank, L. M., Howell, S., Clarke, A. D., Freitag, S., Brekhovskikh, V., Kapustin, V., … Wood, R. (2012). Organic matter and non-refractory aerosol over the remote Southeast Pacific: Oceanic and combustion sources. *Atmospheric Chemistry and Physics*, *12*(1), 557–576. https://doi.org/10.5194/acp-12-557-2012

Skop, R. A., Viechnicki, J. T., & Brown, J. W. (1994). A model for microbubble scavenging of surface-active lipid molecules from seawater. *Journal of Geophysical Research*, *99*(C8), 16,395–16,402. https://doi.org/10.1029/94JC01199

Smirnov, A., Sayer, A. M., Holben, B. N., Hsu, N. C., Sakerin, S. M., Macke, A., … Radionov, V. F. (2012). Effect of wind speed on aerosol optical depth over remote oceans, based on data from the maritime aerosol network. *Atmospheric Measurement Techniques*, *5*(2), 377–388. https://doi.org/10.5194/amt-5-377-2012

Stefan, R. L., & Szeri, A. J. (1999). Surfactant scavenging and surface deposition by rising bubbles. *Journal of Colloid and Interface Science*, *212*(1), 1–13. https://doi.org/10.1006/jcis.1998.6037

Stokes, M. D., Deane, G. B., Prather, K., Bertram, T. H., Ruppel, M. J., Ryder, O. S., … Zhao, D. (2013). A marine aerosol reference tank system as a breaking wave analogue for the production of foam and sea-spray aerosols. *Atmospheric Measurement Techniques*, *6*(4), 1085–1094. https://doi.org/10.5194/amt-6-1085-2013

Szumowski, M. J., Rauber, R. M., & Ochs, H. T. (1999). The microphysical structure and evolution of Hawaiian rainband clouds. Part III: A test of the ultragiant nuclei hypothesis. *Journal of the Atmospheric Sciences*, *56*(12), 1980–2003. https://doi.org/10.1175/1520-0469(1999)056%3C1980:TMSAEO%3E2.0.CO;2

Tang, I. N. (1997). Thermodynamic and optical properties of mixed-salt aerosols of atmospheric importance. *Journal of Geophysical Research*, *102*(D2), 1883–1893. https://doi.org/10.1029/96JD03085

Tang, I. N., Tridico, A. C., & Fung, K. H. (1997). Thermodynamic and optical properties of sea salt aerosols. *Journal of Geophysical Research*, *102*(D19), 23,269–23,275. https://doi.org/10.1029/97JD01806

Terrill, E. J., Melville, W. K., & Stramski, D. (2001). Bubble entrainment by breaking waves and their influence on optical scattering in the upper ocean. *Journal of Geophysical Research*, *106*(C8), 16,815–16,823. https://doi.org/10.1029/2000JC000496

Textor, C., Schulz, M., Guibert, S., Kinne, S., Balkanski, Y., Bauer, S., … Chin, M. (2006). Analysis and quantification of the diversities of aerosol life cycles within AeroCom. *Atmospheric Chemistry and Physics*, *6*(7), 1777–1813. https://doi.org/10.5194/acp-6-1777-2006

Thorpe, S. A. (1982). On the cloud of bubbles formed by a breaking wind-wave in deep water, and their role in air-sea gas transfer. *Philosophical Transactions of the Royal Society of London*, *304A*, 155–210.

Thorpe, S. A., & Hall, A. J. (1983). The characteristics of breaking waves, bubble clouds, and near-surface currents observed using side-scan sonar. *Continental Shelf Research*, *1*(4), 353–384. https://doi.org/10.1016/0278-4343(83)90003-1

Thorpe, S. A., Stubbs, A. R., Hall, A. J., & Turner, R. J. (1982). Wave-produced bubbles observed by side-scan sonar. *Nature*, *296*(5858), 636–638. https://doi.org/10.1038/296636a0

Turekian, V. C., Macko, S. A., & Keene, W. C. (2003). Concentrations, isotopic compositions, and sources of size-resolved, particulate organic carbon and oxalate in near-surface marine air at Bermuda during spring. *Journal of Geophysical Research, 108*(D5), 4157. https://doi.org/10.1029/2002JD002053

Tyree, C. A., Hellion, V. M., Alexandrova, O. A., & Allen, J. O. (2007). Foam droplets generated from natural and artificial seawaters. *Journal of Geophysical Research*, *112*, D12204. https://doi.org/10.1029/2006JD007729

Vignati, E., de Leeuw, G., & Berkowicz, R. (2001). Modeling coastal aerosol transport and effects of surf-produced aerosols on processes in the marine atmospheric boundary layer. *Journal of Geophysical Research*, *106*(D17), 20,225–20,238. https://doi.org/10.1029/2000JD000025

Woodcock, A. H. (1952). Atmospheric seasalt particles and raindrops. *Journal of Meteorology*, *9*(3), 200–212. https://doi.org/10.1175/1520-0469(1952)009%3C0200:ASPAR%3E2.0.CO;2

Woodcock, A. H. (1953). Salt nuclei in marine air as a function of altitude and wind force. *Journal of Meteorology*, *10*(5), 362–371. https://doi.org/10.1175/1520-0469(1953)010%3C0366:SNIMAA%3E2.0.CO;2

Woodcock, A. H., & Gifford, M. M. (1949). Sampling atmospheric sea salt nuclei over the ocean. *Journal of Marine Research*, *8*, 177.

Zhang, J., & Reid, J. S. (2006). MODIS aerosol product analysis for data assimilation: Assessment of over-ocean level 2 aerosol optical thickness retrievals. *Journal of Geophysical Research*, *111*, D22207. https://doi.org/10.1029/2005JD006898

Zhou, X., Davis, A. J., Kieber, D. J., Keene, W. C., Maben, J. R., Maring, H., … Smoydzyn, L. (2008). Photochemical production of hydroxyl radical and hydroperoxides in water extracts of nascent marine aerosols produced by bursting bubbles from Sargasso seawater. *Geophysical Research Letters*, *35*, L20803. https://doi.org/10.1029/2008GL035418